

# Multiwavelength modeling the SED of Luminous Supersoft X-ray Sources in Large Magellanic Cloud and Small Magellanic Cloud

AUGUSTIN SKOPAL<sup>1</sup>

<sup>1</sup>*Astronomical Institute, Slovak Academy of Sciences,  
059 60 Tatranská Lomnica, Slovakia*

## ABSTRACT

Classical supersoft X-ray sources (SSSs) are understood as close binary systems in which a massive white dwarf (WD) accretes from its companion at rates sustaining a steady hydrogen burning on its surface generating bolometric luminosities of  $10^{36} - 2 \times 10^{38} \text{ erg s}^{-1}$ . Here, we perform for the first time the global supersoft X-rays to near-infrared (NIR) spectral energy distribution (SED) for the brightest SSSs in LMC and SMC. We test a model in which the ultraviolet–NIR is dominated by emission from a compact (unresolved) circumstellar nebula represented by the ionized gas out-flowing from the SSS. The SED models correspond to luminosities of SSSs of a few times  $10^{38} - 10^{39} \text{ erg s}^{-1}$ , radiating at blackbody temperatures of  $\approx 3 \times 10^5 \text{ K}$ , and indicate nebular continuum, whose emission measure of  $\gtrsim 2 \times 10^{60} \text{ cm}^{-3}$  corresponds to a wind mass-loss at rates  $\gtrsim 2 \times 10^{-6} M_{\odot} \text{ yr}^{-1}$ . Such the extreme parameters suggest that the brightest SSSs could be unidentified optical novae in a post-nova SSS state sustained at a high long-lasting luminosity by resumed accretion, possibly at super-Eddington rates. New observations and theoretical multiwavelength modeling of the global SED of SSSs are needed to reliably determine their parameters, and thus to understand their proper stage in stellar evolution.

*Keywords:* Fundamental parameters of stars — X-rays: binaries — X-rays: individual: (RX J0513.9-6951, RX J0058.6-7135, RX J0543.6-6822, RX J0527.8-6954)

## 1. INTRODUCTION

Luminous supersoft X-ray sources (SSSs) were discovered in the Large Magellanic Cloud (LMC) and in the Small Magellanic Cloud (SMC) by Long et al. (1981) and Seward & Mitchell (1981). They are characterized by very soft thermal spectra, emitting predominantly at energies  $\lesssim 0.5 \text{ keV}$  (Greiner et al. 1991). Their extremely soft spectra correspond to blackbody temperatures of  $\approx 15\text{--}80 \text{ eV}$  and bolometric luminosities of  $10^{36} - 2 \times 10^{38} \text{ erg s}^{-1}$ . These objects are commonly accepted as binaries that consist of a massive white dwarf (WD) radiating close to the Eddington luminosity due to a steady nuclear burning on its surface, when the hydrogen-rich material is burned as fast as it is accreted, at rates of the order of  $10^{-7} M_{\odot} \text{ yr}^{-1}$  (van den Heuvel et al. 1992; Kahabka & van den Heuvel 1997). Following multiwavelength observations have revealed a significant excess of the radiation in the ultraviolet (UV) to near-infrared (NIR), well above the Rayleigh-Jeans tail of the SSS radiation itself (see Sects. 1.1 – 1.4 and 2). To explain the high luminosity of bright SSSs, and the

longer wavelength excess, Popham & di Stefano (1996) proposed a model, in which a significant fraction of the WD’s radiation is converted to the UV–NIR by irradiating, (i) the flared accretion disk and (ii) the donor star.

In this paper we selected four bright SSSs observed in the Magellanic Clouds, RX J0513.9-6951, RX J0058.6-7135, RX J0543.6-6822 and RX J0527.8-6954, with the aim to model their global X-ray–NIR spectral energy distribution (SED) by the method of multiwavelength modeling described by Skopal (2015). The motivation for this work is the absence of the SED model, which would uniformly fit radiation of SSSs in both the supersoft X-ray and the UV–NIR domains. Further, the extreme properties of SSSs and their spectral features indicate the presence of the nebular radiation in the spectrum (see Appendix A), which could explain the observed strong UV–NIR excess as it is currently considered for the accreting nuclear-burning WDs in symbiotic binaries (Kenyon & Webbink 1984; Muerset et al. 1991; Skopal 2005). Therefore, here we are testing SED modeling, in which the UV–NIR is dominated by the nebular

emission instead of the irradiated disk/companion radiation.

Section 2 summarizes the observed supersoft X-rays to NIR SED of our targets, while Sect. 3 introduces the method and results of our analysis. Their discussion is found in Sect. 4, while Sect. 5 summarizes our findings, and proposes tasks for future investigation. In the following subsections, we first introduce our targets.

### 1.1. *The LMC SSS RX J0513.9-6951*

RX J0513.9-6951 is a transient binary supersoft X-ray source. Currently, it is thought that the system contains a somewhat evolved star and a relatively massive compact object at a 0.76-day orbit, viewed nearly pole-on (Crampton et al. 1996; Southwell et al. 1996). The system is the brightens SSS emitting a significant amount of the radiation also in the far-UV ( $\gtrsim 10^{-13}$  erg cm $^{-2}$  s $^{-1}$  Å $^{-1}$ ).

RX J0513.9-6951 was discovered during the *ROSAT* All-sky Survey (1990 July – 1991 January) in the LMC (Schaeidt et al. 1993). The authors found it to be variable and matched its total average spectrum by a blackbody radiation (see Table 1). Pakull et al. (1993) revealed the optical counterpart as a  $B \approx 17$  mag blue star. Its spectrum was dominated by the hydrogen Balmer lines with a signature of a broad P-Cyg absorption component indicating a mass-loss from the system at  $v_\infty \approx 3600$  km s $^{-1}$ . Absence of He I lines and the presence of highly ionized ions (O VI 3811, 3834 doublet, He II) with  $I_{\text{He II } 4686} \gg I_{\text{H}\beta}$  reflect the presence of a very hot ionizing source in the binary. They also pointed that the optical counterpart appears fainter during the X-ray outburst.

Pronounced optical variability of RX J0513.9-6951 was revealed by optical multicolor monitoring campaigns. Reinsch et al. (1996) measured an optical low states during February to December, 1993, lasting around 40 days with a decrease in the continuum by  $\Delta V \sim 1$  mag and a factor of  $\approx 10$  decrease in emission line fluxes. The light curve obtained within the MA-CHO project specified the occurrence of the low stages on a time-scale of  $\sim 100 - 200$  days (Alcock et al. 1996; Southwell et al. 1996). In addition, during the high-state, these authors revealed a small ( $\Delta V \sim 0.05$ ) light modulation with a period of 0.763 d, which is consistent with variations in the radial velocities of He II  $\lambda 4686$  emission line, and thus confirms a binary nature of the system (Crampton et al. 1996).

Broad wings of the strongest emission lines (He II and H $\beta$ ) accompanied with satellite components indicated a bipolar outflow and thus the presence of a disk in the binary. The bipolar outflow in the form of jets sug-

gested that the accretor is a WD (Southwell et al. 1996; Crampton et al. 1996).

Based on all previously published optical and X-ray data, Southwell et al. (1996) pointed out the principal feature of the variability: the anti-correlation between the supersoft X-ray and the optical fluxes. X-ray monitoring of RX J0513.9-6951 showed that the flux anti-correlation is very strict: There are cyclic changes between optical-low/X-ray-on states and optical-high/X-ray-off states (e.g., Reinsch et al. 2000; Charles et al. 2010).

Based on the *HST* ultraviolet spectroscopy, Gänsicke et al. (1998) derived the neutral hydrogen density  $N_{\text{H}} = (5.5 \pm 1.0) \times 10^{20}$  cm $^{-3}$ . The authors found that this value is consistent with parameters determined by model atmosphere fits to the *ROSAT* PSPC spectrum of July 1993 (see Table 1).

### 1.2. *The SMC SSS RX J0058.6-7135 (LIN 333)*

Henize (1956) labeled this object in his “Catalog of Emission Nebulae in the Small Cloud” as LH $\alpha$ -115 N67. Independently, Lindsay (1961) put it in his catalog under the number 333, remarking features of a planetary nebula in its spectrum. Therefore, the identifier LIN 333 is frequently used for this object. Aller et al. (1987) analyzed its *IUE* spectra, and revealed a strong nebular emission produced by the object, characterized with the emission measure of  $\sim 1.4 \times 10^{60}$  cm $^{-3}$  (see Appendix A) and a high electron temperature of  $\sim 30\,000$  K. They also measured the optical position of the nebula, which helped Wang (1991) to identify LH $\alpha$ -115 N67 with the strong SSS 1E0056.8-7154, which is also named as SMP SMC 22 (Sanduleak et al. 1978). Wang (1991) suggested that 1E0056.8-7154 is the single hot nucleus of the planetary nebula LH $\alpha$ -115 N67. The X-ray detection of this source was first reported by Seward & Mitchell (1981) on the basis of observations with the *Einstein* satellite. Following X-ray observations were carried out by the *ROSAT* and *XMM-Newton* satellites, see Kahabka et al. (1994) and Mereghetti et al. (2010), respectively. Modeling the X-ray SED of LIN 333 was performed by Kahabka et al. (1994), Heise et al. (1994), and Mereghetti et al. (2010). Corresponding parameters are introduced in Table 1. Based on their models, Heise et al. (1994) found that accreting WD in a binary is consistent with the *ROSAT* spectrum of 1E0056.8-7154, but also admitted a possibility that the SSS is an exceptionally hot single central star of a planetary nebula. Comparing all X-ray data and their models, spanning almost 30 years, Mereghetti et al. (2010) did not find any apparent long-term variability in the luminosity or spectrum of

LIN 333. The authors pointed out that the lack of variability, typical for other SSSs, and too low upper limit to the optical counterpart ( $V \sim 21$ , Villaver et al. 2004) do not favor a binary nature of LIN 333. Therefore, they supported the interpretation that it is a single, very hot star on its way to becoming a relatively massive ( $\sim 1 M_{\odot}$ ) WD. Using the *Spitzer Space Telescope* infrared spectra, Bernard-Salas et al. (2009) classified SMP SMC 22 as a high-excitation planetary nebula with high excitation lines ([O IV] and [Ne V]). The absence of dust-related features in the spectrum was ascribed to the high temperature and luminosity of SMP SMC 22.

In spite of these arguments, we interpret the results of our multiwavelength modeling of the LIN 333 SED within a binary-star model, in which a WD accretes from its companion at a high rate (Sect. 4.3). The main reason for this assumption is the exceptionally high luminosity of LIN 333 compared to other planetary nebulae, indication of a compact unresolved nebula in its spectrum – common main features of all our targets (Fig. 1, Sect. 4.5, Appendix A), and possible presence of the binary companion indicated by the optical fluxes (see Appendix C).

### 1.3. The LMC SSS RX J0543.6-6822 (CAL 83)

The bright SSS CAL 83 was discovered in the *Einstein* survey of the LMC (Long et al. 1981). Subsequent observations with *EXOSAT* from November 1983 confirmed its very soft X-ray spectrum with an upper limit of 0.3 count/s (Pakull et al. 1985). The optical spectrum from May 1984 revealed its similarity to that of the low mass X-ray binaries LMC X-2 and Sco X-1. From radial velocity variations of the optical emission lines (H and He II  $\lambda 4686$ ), Crampton et al. (1987) discovered that CAL 83 is a binary system with a period of  $\sim 1$  day. Orbital elements from radial velocities of the He II  $\lambda 4686$  line were improved by Schmidtke et al. (2004).

Following X-ray observations of CAL 83 were carried out with the *ROSAT*, *BeppoSAX*, *Chandra* and *XMM-Newton* satellites. Kahabka (1998) presented a 1.5-year X-ray light curve of CAL 83 as measured with the *ROSAT/HRI* from July 1995 to December 1996. The authors also indicated the first short-term X-ray-off state of CAL 83 on JD 2450200 (April 26, 1996). The second and the third X-ray-off state was reported by Greiner & Di Stefano (2002) and Lanz et al. (2005) on the basis of *Chandra* observations from November 1999 and October 2001, respectively. This demonstrates recurrent nature for CAL 83. Modeling the X-ray SED of CAL 83 was carried out by Greiner et al. (1991), Kahabka (1998), Parmar et al. (1998), Paerels et al.

(2001) and Lanz et al. (2005). Corresponding parameters are found in Table 1.

The prototypical SSS CAL 83 was also intensively studied in the ultraviolet and optical. It was identified with a variable, blue,  $V \approx 17$ , point like source with an orbital period of 1.047 days (Cowley et al. 1984; Pakull et al. 1985; Smale et al. 1988; Schmidtke et al. 2004; Rajoelimanana et al. 2013). Optical 3900–6800 Å spectrum from May 1984 showed relatively weak Balmer emission lines and a high He II  $\lambda 4686/H\beta$  ratio ( $> 5$ ). The nebular [O III] 5007 Å line was also present. The blue-shifted He II  $\lambda 4686$  emission component suggested a mass outflow with velocities at 1500–2300 km s<sup>-1</sup> (Pakull et al. 1985). CAL 83 is known to show irregular brightness variations of more than a magnitude over timescales of months. Using the MACHO *V* and *R* light curves (1993–1999), Greiner & Di Stefano (2002) indicated that CAL 83 exhibits distinct and well-defined low, intermediate, and high optical states, characterized with no color changes during transition phases. They also found that X-ray-off states were observed during optical high states. A variability has also been found in the ultraviolet by Gänsicke et al. (1996), who observed CAL 83 during high and low states. More recent optical and X-ray observations revealed a quasi-periodic variation on a time-scale of 450 d with the optical low and high states lasting for  $\sim 200$  and  $\sim 250$  d (Rajoelimanana et al. 2013). The authors also clearly established the X-ray/optical flux anticorrelation. It was found that the X-ray light curve exhibits significant modulations with periodicities from 67 s to hours (Odendaal et al. 2014; Odendaal & Meintjes 2017). It is generally assumed that variations in the optical flux are most likely associated with changes in the accretion disk (e.g., Greiner & Di Stefano 2002).

Optical imaging of CAL 83 revealed the presence of an extended ionized nebula surrounding CAL 83, first recognized by Pakull & Motch (1989) on the [O III]  $\lambda 5007$  CCD image with a diameter of  $\sim 50''$ . Remillard et al. (1995) reported that the nebula is caused by the illumination of the local ISM by the central SSS CAL 83 with the time-averaged X-ray luminosity  $> 3 \times 10^{37}$  erg s<sup>-1</sup>. The authors inferred that the nebula has a bright inner zone with a characteristic radius, particle density and mass of  $\sim 7.5$  pc,  $4\text{--}10$  cm<sup>-3</sup> and  $\gtrsim 150 M_{\odot}$ , respectively, while the diffuse outer nebula has a characteristic radius of  $\sim 20$  pc. Based on the spectra taken over a  $25'' \times 25''$  field of view (FoV, i.e.,  $7.5 \times 7.5$  pc<sup>2</sup> for the distance of 55 kpc), Gruyters et al. (2012) presented the morphology of the ionized gas within the inner nebula, for the first time indicated there a He II  $\lambda 4686$  emission region, and extracted the global spectrum of the ionization neb-

**Table 1.** Physical parameters of our targets from the literature (designation as in Sect. 3.1)

Object	$N_{\text{H}}$ [ $10^{20} \text{ cm}^{-2}$ ]	$R_{\text{SSS}}^{\text{eff}}$ [ $R_{\odot}$ ]	$T_{\text{BB}}/T_{\text{eff}}$ [ K ]	$\log(L_{\text{SSS}})$ [ $\text{erg s}^{-1}$ ]	Model BB/Atm.	Ref.
RX J0513	9.4	$\sim 0.039$	$456000 \pm 78000$	$\sim 38.37$	BB <sup>a</sup>	1
RX J0513	4–7	0.009–0.017	$\approx 560000$	37.40–37.95	Atm. <sup>b</sup>	2
LIN 333	5.2 - 16	0.086	160000 - 400000	38.28	BB <sup>l</sup>	9
LIN 333	5	0.012	440000	37.30	Atm. <sup>c</sup>	3
LIN 333	8	0.072	360000	38.48	BB <sup>c</sup>	3
LIN 333	2.8–3.2	0.19–0.22	154000	37.81–37.93	Atm. <sup>d</sup>	4
LIN 333	5.2	0.049	313000	37.91	BB <sup>d</sup>	4
CAL 83	17	$> 0.06$	302000	$L_{\text{SSS}} > L_{\text{Edd}}$	BB <sup>e</sup>	5
CAL 83	8	0.022	500000	$L_{\text{SSS}} \equiv L_{\text{Edd}}$	BB <sup>f</sup>	5
CAL 83	8.87	0.014–0.016	516000	37.76	Atm. <sup>g</sup>	6
CAL 83	6.07	$\gtrsim 0.015$	$\lesssim 403000$	$\gtrsim 37.30$	Atm. <sup>g</sup>	6
CAL 83	6.5	$0.012 \pm 0.003$	$539000 \pm 16000$	$37.40 \pm 0.03$	BB <sup>h</sup>	7
CAL 83	6.5	$0.018 \pm 0.001$	$378000 \pm 9000$	$37.37 \pm 0.01$	Atm. <sup>h</sup>	7
CAL 83	$6.5 \pm 1.0$	$0.01 \pm 0.001$	$550000 \pm 25000$	$37.54 \pm 0.13$	Atm. <sup>i</sup>	8
RX J0527	14	$> 0.16$	209000	$L_{\text{SSS}} > L_{\text{Edd}}$	BB <sup>j</sup>	5
RX J0527	8.5	0.043	348000	$L_{\text{SSS}} \equiv L_{\text{Edd}}$	BB <sup>k</sup>	5

<sup>a</sup> ROSAT, October 30, 1990; 1 - Schaeidt et al. (1993); <sup>b</sup> ROSAT, July 1993; 2 - Gänsicke et al. (1998); <sup>c</sup> ROSAT, October 8, 1991; 3 - Heise et al. (1994); <sup>d</sup> XMM-Newton, dates in Table 2; 4 - Mereghetti et al. (2010); <sup>e</sup> ROSAT, June 20, 1990 - best fit; 5 - Greiner et al. (1991); <sup>f</sup> as in <sup>e</sup>, but for the Eddington luminosity ( $L_{\text{Edd}}$ ); <sup>g</sup> ROSAT, observation No. 500131p; 6 - Kahabka (1998); <sup>h</sup> BeppoSAX,  $N_{\text{H}}$  fixed, March 7-8, 1997; 7 - Parmar et al. (1998); <sup>i</sup> Chandra, XMM-Newton,  $N_{\text{H}}$  fixed, dates in Table 2; 8 - Lanz et al. (2005); <sup>j</sup> ROSAT, June 16-25, 1990 - best fit; <sup>k</sup> as in <sup>j</sup>, but for  $L_{\text{Edd}}$ ; <sup>l</sup> ROSAT, October 27-31, 1990; 9 - Kahabka et al. (1994).

ula within their FoV (see Appendix B, in detail). Using the CLOUDY software and typical parameters of a SSS, the authors modeled the CAL 83 nebula. However, none of their models was able to fit the observed spectrum very well. It is of interest to note that searching for ionization nebulae surrounding other strong SSSs in LMC and SMC has been negative, which indicates that either the ISM densities in their environments must be significantly lower than surrounding CAL 83, or the average X-ray luminosities of these sources over the last  $\lesssim 10000$  years must be significantly lower than presently observed (Woods & Gilfanov 2016; Farias et al. 2020).

#### 1.4. The LMC SSS RX J0527.8-6954

This source was discovered during the calibration phase of ROSAT pointing the LMC field between 16 and 25 June 1990 (Greiner et al. 1991). Profile of its supersoft spectrum was very similar to that of CAL 83, but it was fainter by a factor of  $\sim 10$ . The model SED was done by Greiner et al. (1991) (Table 1).

Repeated observations of this source exhibited a continuous decline in the photon counts, from  $\sim 0.2$  to  $\sim 0.01 \text{ cts s}^{-1}$ , during 1990 to 1995 (Greiner et al. 1996).

The authors speculated that a likely mechanism causing the X-ray variability could be a hydrogen flash on a massive WD ( $\geq 1.1 M_{\odot}$ ) accreting at a high rate of  $10^{-7} M_{\odot} \text{ yr}^{-1}$ . This view is supported by the fact that the source was not detected by the *Einstein* satellite 20 years ago, which thus appears that the source is recurrent and was in a declining phase during the ROSAT observations. Also the 4-yr light curve revealed a steady fading by  $\lesssim 0.5 \text{ mag}$  and a 0.39-day modulation with  $\sim 0.05 \text{ mag}$  semi-amplitude.

Based on the optical photometry obtained via the MACHO project, Alcock et al. (1997) first suggested an optical counterpart to RX J0527.8-6954, and Cowley et al. (1997) specified it as a B8IV star with  $V = 17.3 \text{ mag}$ . Using a high-resolution imaging, Oliveira et al. (2010) identified the X-ray source with a B5e V star that is associated with a bipolar H $\alpha$  subarc-second extended emission. The authors pointed that for a massive WD and the Be V companion with  $M \sim 6 M_{\odot}$ , the orbital period has to exceed 21 hours, and thus the 0.39-day period cannot be associated with the orbit.

## 2. OBSERVATIONS

**Table 2.** Log of the used observations from the space

Date yyyy/mm/dd	Julian date JD 2 4...	Region [nm]	Observing satellite	$T_{\text{exp}}$ [ks]
RX J0513.9-6951				
1990/10/30 <sup>1</sup>	48195.5	1.92–6.2	<i>ROSAT</i> <sup>2</sup>	1.9
2001/10/31	52214.5	94–118	<i>FUSE</i> <sup>3</sup>	6.6
2003/07/05	52827.0	94–118	<i>FUSE</i> <sup>3</sup>	33.0
1996/11/13	50401.7	115–144	<i>HST</i> <sup>3</sup>	2.8
1992/04/24	48736.6	115–198	<i>IUE</i> <sup>3</sup>	24.0
1992/04/25	48737.6	186–335	<i>IUE</i> <sup>3</sup>	23.0
1995/06/29	49898.4	115–198	<i>IUE</i> <sup>4</sup>	22.8
RX J0058.6-7135 (LIN 333)				
1991/10/08	48537.5	2.5–6.2	<i>ROSAT</i>	17
2007/06/04	54256.8	2.5–6.3	<i>XMM-Newton</i>	7.7
2009/05/14	54966.3	2.5–6.3	<i>XMM-Newton</i>	16.54
2009/09/25	55100.3	2.5–6.3	<i>XMM-Newton</i>	32.3
2002/07/25	52480.5	92–119	<i>FUSE</i>	26.4
1984/04/16	45806.5	150 - 190	<i>IUE</i>	14
1984/04/17	45807.5	190 - 333	<i>IUE</i>	16
1995/03/20	49796.5	150 - 540	<i>HST</i>	2.5
RX J0543.6-6822 (CAL 83)				
1990/06/20	48063.5	2.1–5.9	<i>ROSAT</i>	3.6
2000/04/23	51658.0	2.4–5.4	<i>XMM-Newton</i>	45.1
2001/08/15	52137.3	2.4–5.4	<i>Chandra</i>	35.4
2001/09/22	52175.3	93.5–118	<i>FUSE</i>	45.6
1996/11/10	50398.0	115–144	<i>HST</i>	2.8
1984/11/24	46029.1	115–198	<i>IUE</i>	15.1
1987/12/12	47142.0	115–198	<i>IUE</i>	14.4
1990/10/29	48194.1	115–198	<i>IUE</i>	24.4
1990/11/07	48203.4	115–198	<i>IUE</i>	22.8
1987/12/11	47141.0	186–332	<i>IUE</i>	16.1
1988/08/12	47397.3	197–333	<i>IUE</i>	12.9
RX J0527.8-6954				
1990/06/20	48063.5	2.6–5.9	<i>ROSAT</i>	18.8
1992/09/01	48867.2	115–198	<i>IUE</i>	16.7
1992/09/01	48867.3	240–318	<i>IUE</i>	6.0

<sup>1</sup> average of the second part, <sup>2</sup> the total spectrum (see Fig. 2 of [Schaeidt et al. 1993](#)), <sup>3</sup> high state, <sup>4</sup> low state.

This section summarizes observations of our targets we used to model their global SED in the continuum. Spectroscopic observations with *Far Ultraviolet Spectroscopic Explorer (FUSE)*, *Hubble Space Telescope (HST)* and *International Ultraviolet Explorer (IUE)* were obtained from the satellite archives with the aid of the MAST. Other observations were taken from the literature and catalogs as referred in the following subsections. Data obtained from the space are collected in Table 2. Stellar magnitudes in the optical–NIR

were converted to fluxes according to the calibration of [Henden & Kaitchuck \(1982\)](#) and [Bessell \(1979\)](#). To correct the observed X-ray fluxes for absorptions we used the *tbabs* absorption model for the interstellar matter composition with abundances given by [Wilms et al. \(2000\)](#) (e.g.,  $\log(A_{\text{OI}}) + 12 = 8.69$ ). Observations for  $\lambda > 912 \text{ \AA}$  were dereddened with  $E_{\text{B-V}} = 0.06$  and 0.08 (unless otherwise specified), and physical parameters were scaled with the distance  $d = 49$  and 60 kpc

to objects in the LMC and SMC, respectively (Mateo 1998).

### 2.1. *RX J0513.9-6951*

The observed SED of RX J0513.9-6951, used in this contribution, covers the spectral range from 1.92 nm to 2200 nm. It consists of the *ROSAT PSPC* observations (1.92 – 6.20 nm) as published by Schaeidt et al. (1993). The data were adopted from their figure 2. The far-UV spectra with *FUSE* (B0160104, D0060102) were taken during the high state of RX J0513.9-6951 as found by Hutchings et al. (2002) for the 2001 observation, and according to the light curve of Burwitz et al. (2008) for the 2003 spectrum. The average continuum level of both spectra is comparable, with  $F(2001)/F(2003) \sim 1.2$ . According to the light curve of Cowley et al. (2002), the high resolution *HST/GHRS* spectrum (Z3HS0205T) was also taken during a high state. Further spectroscopic observation in the ultraviolet was carried out with the *IUE* satellite. The 1992 spectrum (SWP44467, LWP22883) corresponds to a high state, because its short-wavelength part fits well the *HST* spectrum. However, the 1995 spectrum (SWP55170) was taken at the optical minimum, i.e., during a low state (Cowley et al. 2002).

Observations from the space were supplemented with the ground-based optical spectroscopy obtained during both the high state (Pakull et al. 1993) and the low state (Reinsch et al. 1996). The former was taken nearly simultaneously with the *IUE* high-state spectra from 1992. In addition, optical *BVR* broad-band photometry was estimated from Fig. 1 of Reinsch et al. (1996). Further *RI* and infrared *JHK* photometric measurements were found in the USNO-B1.0 Catalog ( $R = 16.54$ ,  $I = 15.75$ ) (Monet et al. 2003), the NOMAD Catalog ( $V = 16.640$ ,  $R = 16.540$ ) (Zacharias et al. 2005), and the 2MASS All-Sky Catalog of Point Sources ( $J = 16.492 \pm 0.157$ ,  $H \sim 15.517$ ,  $K \sim 15.728$ ) (Skrutskie et al. 2006).

### 2.2. *RX J0058.6-7135 (LIN 333)*

Multiwavelength observations, we used to model the SED of this SSS, cover the spectral range from the supersoft X-rays to the optical ( $\sim 2.4 - 360$  nm). The supersoft X-ray fluxes made by the *ROSAT* satellite were reconstructed with the aid of Fig. 2 in Heise et al. (1994), and those carried out with the *XMM-Newton* satellite were estimated according to the blackbody model of Mereghetti et al. (2010). The ultraviolet spectra were obtained from the satellite archives of *FUSE* (C0560301000), *IUE* (SWP22766, LWP3168) and *HST FOS* (Y2N30104T, Y2N30105T, Y2N30106T). Spectroscopic observations were supplemented with the *UBVR*

broad-band photometry, taken from the catalogs of Massey (2002) ( $U = 16.16$ ,  $B = 16.86$ ,  $V = 16.37$ ,  $R = 16.09$ ), Zaritsky et al. (2002) ( $U = 16.643$ ,  $B = 17.240$ ,  $V = 16.924$ ), Skiff (2010) ( $V = 16.90$ ), and the 3rd release of the *DENIS* catalog ( $I = 17.662$ ,  $J = 16.156$ ).

### 2.3. *RX J0543.6-6822 (CAL 83)*

The observed SED of CAL 83, used in this paper, covers the spectral range from 2.07 nm to 790 nm. The calibrated supersoft X-ray fluxes were reconstructed from Fig. 1 of Greiner et al. (1991) (*ROSAT*) and Fig. 1 of Lanz et al. (2005) (*Chandra*, *XMM-Newton*). In both cases the source was in the X-ray-on state (see Kahabka 1998, for the *ROSAT* observation).

In the ultraviolet, eleven far-UV spectra of CAL 83 were carried out by *FUSE* (B0150101) on September 22, 2001 (Schmidtke et al. 2004). The continuum fluxes were estimated within the range of 93.5 – 118 nm. The high resolution *HST/GHRS* spectrum (Z3HS0105T) covers the region from  $\sim 114.9$  to  $\sim 143.5$  nm. Further spectroscopic observation in the ultraviolet was carried out with the *IUE* satellite. Continuum of the SWP spectra No. 24554, 32511, 39995, 40075 and the LWP spectra No. 12257, 13902 were consistent best with those of the *HST* and *FUSE* spectra. Therefore, we used their average fluxes weighted with exposure times to model the SED. Other *IUE* spectra had a higher continuum, in particular the SWP30024 spectrum was a factor of  $> 2$  above the used minimum values. According to the measured variations in both the X-ray and the UV-optical fluxes and their anticorrelation (see Greiner & Di Stefano 2002), it is probable that the minimum level of the UV continuum, which we used to model the SED, corresponds to the X-ray-on phase of CAL 83.

Spectroscopic observations were supplemented with the optical *UBVRI* broad-band photometry, taken from catalogs of Massey (2002) ( $U = 16.25$ ,  $B = 17.18$ ,  $V = 17.44$ ), Zaritsky et al. (2004) ( $U = 16.022$ ,  $B = 16.864$ ,  $V = 16.976$ ) and the 3rd release of the *DENIS* database ( $R = 17.0$ ,  $I = 16.538$ ). Compared are values reported by Crampton et al. (1987) ( $B = 17.19 - 17.34$ ,  $V = 17.22 - 17.35$ ), and fluxes from the optical, 400–680 nm, spectrum published by Pakull et al. (1985) scaled with their average photometric measurements ( $U - B = -1.04 \pm 0.06$ ,  $B - V = 0.02 \pm 0.06$ ,  $B = 17.2 \pm 0.3$ ). In the near-IR Kato et al. (2007) measured  $J = 16.98$ ,  $H = 16.81$  and  $K = 16.77$ , and 2MASS 6X Point Source Working Database/Catalog reports  $J = 17.433$ ,  $H = 17.016$  and  $K = 16.079$ .

### 2.4. *RX J0527.8-6954*

In this case, the available observed SED in the continuum covers the spectral range from 2.65 nm to 550 nm.

**Table 3.** Physical parameters of bright SSSs in LMC and SMC from multiwavelength SED models (see Sect. 3.1)

Object	Supersoft X-ray source					Nebula		$\chi^2_{\text{red}}/\text{d.o.f.}$
	$N_{\text{H}}$ [ $10^{20} \text{ cm}^{-2}$ ]	$R_{\text{SSS}}^{\text{eff}}$ [ $R_{\odot}$ ]	$T_{\text{BB}}$ [K]	$\log(L_{\text{SSS}})$ [ $\text{erg s}^{-1}$ ]	$\log(L_{\text{X}})^7$ [ $\text{erg s}^{-1}$ ]	$T_{\text{e}}$ [K]	$EM$ [ $10^{60} \text{ cm}^{-3}$ ]	
RX J0513 <sup>1</sup>	12±2	0.19±0.02	350000 ± 10000	39.28±0.14	38.25±0.13	30000±10000	2.3±0.2	2.8 / 40
RX J0513 <sup>2</sup>	–	0.26±0.03	350000 <sup>3</sup>	39.54±0.15	38.52±0.14	30000±10000	8.6±0.5	3.6 / 38
LIN 333 <sup>4</sup>	9.0±0.2	0.17±0.02	305000 ± 10000	38.96±0.13	37.66±0.12	37000±5000	1.6±0.2	2.6 / 39
LIN 333 <sup>5</sup>	7.1±0.2	0.18±0.02	267000 ± 7000	38.75±0.12	37.45±0.11	–	–	4.4 / 22
CAL 83 <sup>4</sup>	10.3±0.5	0.15±0.02	345000 ± 15000	39.04±0.16	37.99±0.15	30000±15000	2.9±0.3	3.8 / 61
CAL 83 <sup>6</sup>	12.6±0.5	0.16±0.02	357000 ± 15000	39.14±0.16	38.15±0.15	–	–	2.9 / 35
RX J0527	7.1±0.2	0.16±0.02	255000 ± 20000	38.57±0.06	36.83±0.05	9000±2000	4.3±0.3	3.3 / 34

<sup>1</sup> low state, <sup>2</sup> high state: the  $(1-9) \times 10^3 \text{ \AA}$  model SED for  $T_{\text{h}}$  adapted from the low state (Fig. 2), <sup>3</sup> fixed value, <sup>4</sup> model SED with the *ROSAT* data, <sup>5</sup> model SED with the *XMM-Newton* data, <sup>6</sup> model SED with the *Chandra/XMM-Newton* data, <sup>7</sup> the luminosity in the 0.2–1.0 keV range.

The calibrated supersoft X-ray fluxes were obtained by the *ROSAT* satellite during the pointing observations of the LMC field in 1990 (Greiner et al. 1991). According to Greiner et al. (1996) the source was at the brighter stage.

Ultraviolet spectra of RX J0527.8-6954 were carried out with the *IUE* satellite on September 1, 1992 (SWP45499, LWP23826). The LWP23826 spectrum was underexposed, therefore its part from the short-wavelength edge to  $\sim 240 \text{ nm}$  was not used in the modeling (dotted line in Fig. 1d).

The optical brightness of RX J0527.8-6954 was measured by Cowley et al. (1997) in *UBV* passbands at the Cerro Tololo Inter-American Observatory during December 1992, December 1993 and November 1994. They determined  $V = 17.3$ ,  $B = 17.4$  and  $U = 17.2$ . On September 2004, Oliveira et al. (2010) observed RX J0527.8-6954 using the Gemini South Telescope with the Gemini Multi Object Spectrograph and distinguished the original star into two components. They determined the flux ratio in the *V* band between the components to 1.43, and corrected the *V* magnitude of the RX J0527.8-695 optical counterpart to 17.9.

### 3. ANALYSIS AND RESULTS

#### 3.1. Modeling the SED

The primary aim of this paper is to reconstruct the SED of bright SSSs in LMC and SMC from supersoft X-rays to the optical or NIR. In this way to determine physical parameters of the main components of radiation in the observed continuum. To achieve this aim we use the method of multiwavelength modeling the composite continuum of SSSs described by Skopal (2015). Here we introduce its basic assumptions and relationships.

In our SED modeling the observed continuum,  $F(\lambda)$ , is assumed to consist of a stellar component of radiation,  $F_{\text{SSS}}(\lambda)$ , from the WD pseudo-photosphere, and nebular

continuum,  $F_{\text{N}}(\lambda)$ , from the ionized out-flowing gas (see Appendix A and Sect. 4.4), i.e.,

$$F(\lambda) = F_{\text{SSS}}(\lambda) + F_{\text{N}}(\lambda). \quad (1)$$

In the model we compare the stellar continuum with the blackbody radiation at a temperature  $T_{\text{BB}}$ , while the nebular continuum is approximated by contributions from f–b and f–f transitions in hydrogen plasma radiating at the electron temperature  $T_{\text{e}}$ . In cases, where observations suggest a discontinuity in the continuum around  $\lambda 2050 \text{ \AA}$ , contributions from doubly ionized helium are also included, and the  $\text{He}^{++}$  abundance is set to 0.1. According to Eqs. (6) and (8) of Skopal (2015), Eq. (1) can be expressed in the form,

$$F(\lambda) = \theta_{\text{SSS}}^2 \pi B_{\lambda}(T_{\text{BB}}) e^{-\sigma_{\text{X}}(\lambda) N_{\text{H}}} + k_{\text{N}} \times \varepsilon_{\lambda}(\text{H}, \text{He}^+, T_{\text{e}}), \quad (2)$$

where  $\theta_{\text{SSS}} = R_{\text{SSS}}^{\text{eff}}/d$  is the angular radius of the SSS, given by its effective radius (i.e. the radius of a sphere with the same luminosity) and the distance  $d$ . Attenuation of the light in the X-ray domain is given by the total cross-section for photoelectric absorption per hydrogen atom,  $\sigma_{\text{X}}(\lambda)$  (Cruddace et al. 1974), and the total column density of neutral atoms of hydrogen,  $N_{\text{H}}$  (i.e., given by both the interstellar and circumstellar matter component). The second term at the right is the nebular continuum expressed by its volume emission coefficient  $\varepsilon_{\lambda}(\text{H}, \text{He}^+, T_{\text{e}})$  scaled with the factor  $k_{\text{N}} = EM/4\pi d^2$ , where  $EM = \int_V n_{\text{e}} n^+ dV$  is the emission measure of the nebula given by the electron and a ion concentration,  $n_{\text{e}}$  and  $n^+$ , in the volume  $V$  of the ionized element under consideration. The assumption that the nebular radiation in the continuum can be characterized by a single  $T_{\text{e}}$  is supported by the velocity distribution of free electrons in nebulae that tends to be Maxwellian, because the electrostatic encounters of free electrons are much more likely than any other inelastic scatterings

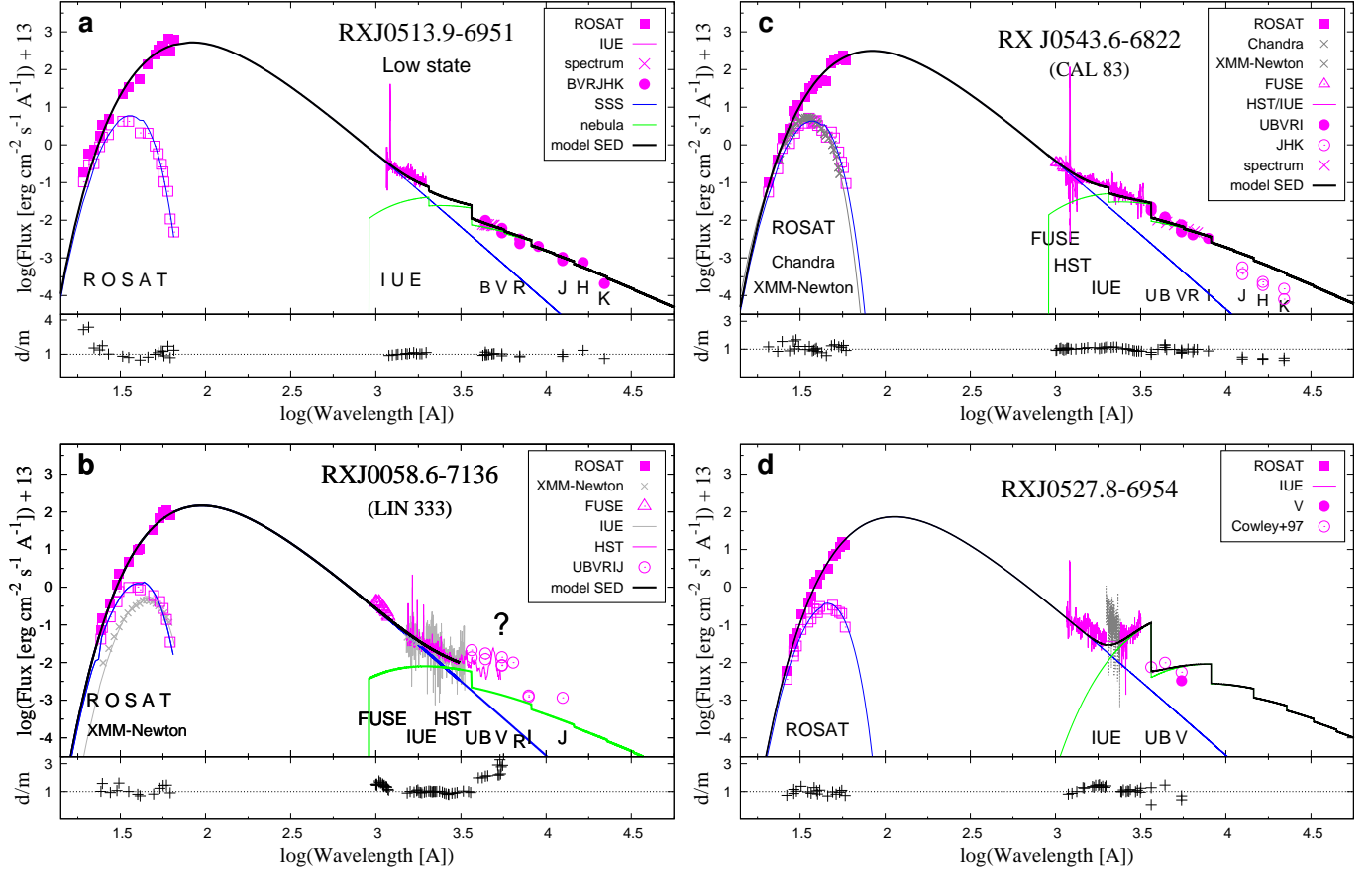


**Figure 1.** A comparison of the measured (in magenta, Sect. 2, Table 2) and model SEDs (heavy black line) of our targets with corresponding data-to-model ratios ( $d/m$ ). Filled/open squares are the unabsorbed/observed X-ray fluxes. The blue and green lines denote components of radiation from the SSS and the nebula, respectively (see Sect. 3, Eq. (2)). **a** – RX J0513.9-6951. **b** – RX J0058.6-7136 (LIN 333): Two models fitting the *ROSAT*–UV and *XMM-Newton*–UV fluxes were performed. *U, B, V, R* fluxes and the optical part of the *HST* spectrum suggest the presence of an additional source of radiation (marked by ?, see Appendix C). **c** – RX J0543.6-6822 (CAL 83): Models performed for the *ROSAT* and *Chandra/XMM-Newton* data (each complemented with the same UV and optical fluxes), are very similar (Table 3). The *J, H, K* fluxes were not used for the modeling. **d** – RX J0527.8-6954: Dotted line is the underexposed part of the LWP23826 spectrum.

(see Bohm & Aller 1947). Therefore, using a single-temperature nebula in the SED modeling expresses the measured UV–NIR fluxes quite well (see the SED models in Skopal 2005, 2015, 2019, and Fig. 1 here). In the modeling procedure we simultaneously fit absorbed X-ray continuum fluxes and dereddened UV to NIR fluxes searching for parameters  $\theta_{\text{SSS}}$ ,  $T_{\text{BB}}$ ,  $N_{\text{H}}$ ,  $T_e$  and  $k_{\text{N}}$  (see Skopal 2015, in detail)<sup>1</sup>. The luminosity of the SSS is calculated as

$$L_{\text{SSS}} = 4\pi d^2 \theta_{\text{SSS}}^2 \sigma T_{\text{BB}}^4. \quad (3)$$

Physical parameters corresponding to our SED models are collected in Table 3.

<sup>1</sup> The corresponding software and application example are available at <https://doi.org/10.5281/zenodo.6985175>

### 3.2. $N_{\text{H}}$ from Rayleigh scattering

The high-resolution *HST/GHRS* spectra ( $\lambda 115$ – $144$  nm) show a pronounced attenuation of the continuum around the Ly- $\alpha$  line that is caused by Rayleigh scattering on atomic hydrogen. This effect can be used to independently determine  $N_{\text{H}}$  in the direction of the SSS (see Sect. 2.3.1 of Skopal 2015). For this purpose we compare the function,

$$F(\lambda) = \theta_{\text{SSS}}^2 \pi B_{\lambda}(T_{\text{BB}}) e^{-\sigma_{\text{Ray}}(\lambda) N_{\text{H}}} + k_{\text{N}} \times \varepsilon_{\lambda}(\text{H}, T_e), \quad (4)$$

to the observed spectrum. The Rayleigh cross-section for scattering by hydrogen in its ground state,  $\sigma_{\text{Ray}}(\lambda)$ , is approximated by Eq. (5) of Nussbaumer et al. (1989). Other parameters have the same meaning as in Eq. (2), and are fixed according to the solution of the global SED.

### 3.3. Multiwavelength model SED of RX J0513.9-6951

Owing to the strict soft X-ray/optical flux anticorrelation, it was possible to perform the X-ray—NIR model SED only for the low state of RX J0513.9-6951 (Fig. 1a), while during the high state, only the far-UV—NIR observations were available to model the corresponding SED (Fig. 2). The best fitting X-ray—NIR model SED parameters,  $N_{\text{H}} = (1.2 \pm 0.2) \times 10^{21} \text{ cm}^{-2}$ ,  $\theta_{\text{SSS}} = 8.8 \times 10^{-14}$  and  $T_{\text{BB}} = (350000 \pm 10000) \text{ K}$ , correspond to a very high luminosity of the SSS source,  $L_{\text{SSS}} = (1.9 \pm 0.7) \times 10^{39} \text{ erg s}^{-1}$ , with the effective radius,  $R_{\text{SSS}}^{\text{eff}} = (0.19 \pm 0.02) R_{\odot}$ . The model SED shows also a significant contribution from the thermal nebula with the emission measure,  $EM = (2.3 \pm 0.2) \times 10^{60} \text{ cm}^{-3}$  that dominates the spectrum for  $\lambda \gtrsim 2000 \text{ \AA}$ .

During the optical-high state, the nebular emission increased by a factor of  $\sim 3.5$  (Table 3), and the WD's effective radius inflated to  $(0.26 \pm 0.03) R_{\odot}$  for the same  $T_{\text{BB}}$  as during the optical-low state. The former suggests that the variable nebular emission is responsible for the optical variability with  $\Delta V \approx 1 \text{ mag}$ , while the latter reflects the increase of the far-UV fluxes of the stellar component of radiation (the blue lines in Fig. 2, see Sect. 4.6 in detail).

Finally, fitting the far-UV *HST/GHRS* spectrum by Eq. (4) we found that the hollow around Ly- $\alpha$  corresponds to  $N_{\text{H}} = (8 \pm 2) \times 10^{20} \text{ cm}^{-2}$ . A comparison of the model SED and the *HST* spectrum constrains the reddening  $E_{\text{B}-\text{V}} = 0.11 \pm 0.02$ . The spectrum and model (4) are shown in Fig. 3.

### 3.4. Multiwavelength model SED of RX J0058.6-7135

Observations of LIN 333 span the wavelength range from supersoft X-rays to the optical. Fluxes in the near-UV and *UBV* bands ( $\sim 1 \times 10^{-15} \text{ erg cm}^{-2} \text{ s}^{-1} \text{ \AA}^{-1}$ , see Fig. 1b), suggest a contribution from the nebula and, possibly, from a companion to the SSS in a binary (see Appendix C). In modeling the supersoft X-ray—optical SED we fitted 13 flux-points between 24 and 62  $\text{\AA}$  and 31 flux-points between 1500 and 3600  $\text{\AA}$  by Eq. (2). Observations with *FUSE* were not used directly in the SED-fitting procedure, because their continuum level is a factor of 1.1–1.5 above that given by the *IUE* and *HST* spectra. Nevertheless, the steep slope of their dereddened fluxes follows the short-wavelength ends of the *IUE* and *HST* spectra, which documents dominant contribution from the SSS to the far-UV (compared are selected fluxes from the LiF2A channel spectrum (1087–1181  $\text{\AA}$ )).

The modeling solution with the *ROSAT* data has the reduced  $\chi^2 = 2.6$ , and corresponds to the fitting parameters of the SSS,  $\theta_{\text{SSS}} = (6.6 \pm 0.7) \times 10^{-14}$ ,  $T_{\text{BB}} =$

$305\,000 \pm 10\,000 \text{ K}$  and  $N_{\text{H}} = (9.0 \pm 0.2) \times 10^{20} \text{ cm}^{-2}$ . These parameters imply the effective radius,  $R_{\text{SSS}}^{\text{eff}} = 0.17 \pm 0.02 (d/60 \text{ kpc}) R_{\odot}$ , and the luminosity,  $L_{\text{SSS}} = 9.1 \pm 3.0 \times 10^{38} (d/60 \text{ kpc})^2 \text{ erg s}^{-1}$ , which translates into the unabsorbed X-ray luminosity  $L_{\text{X}}(0.2 - 1.0 \text{ keV}) = (4.6 \pm 1.6) \times 10^{37} (d/60 \text{ kpc})^2 \text{ erg s}^{-1}$ . Using the average fluxes of the three *XMM-Newton* spectra (see Table 2, Sect. 2.2, Mereghetti et al. 2010) and the same UV—optical fluxes as above, yield the following parameters of the SSS:  $N_{\text{H}} = (7.1 \pm 0.2) \times 10^{20} \text{ cm}^{-2}$ ,  $T_{\text{BB}} = 267\,000 \pm 7\,000 \text{ K}$ ,  $R_{\text{SSS}}^{\text{eff}} = 0.18 \pm 0.02 (d/60 \text{ kpc}) R_{\odot}$  and  $L_{\text{SSS}} = 5.7 \pm 1.8 \times 10^{38} (d/60 \text{ kpc})^2 \text{ erg s}^{-1}$ .

The nebular component of radiation dominates the spectrum from around 2500  $\text{\AA}$  to longer wavelengths (Fig. 1b). Its amount is scaled with  $k_{\text{N}} = 3.8 \pm 0.4 \times 10^{12} \text{ cm}^{-5}$ , which corresponds to  $EM = (1.6 \pm 0.2) \times 10^{60} (d/60 \text{ kpc})^2 \text{ cm}^{-3}$ . The nebula radiates at a high  $T_{\text{e}} = 37\,000 \pm 5\,000 \text{ K}$ . Both,  $EM$  and  $T_{\text{e}}$  are in a good agreement with those derived by Aller et al. (1987) from emission lines:  $EM \sim 1.8 \times 10^{60} (d/63.1 \text{ kpc})^2 \text{ cm}^{-3}$ ,  $T_{\text{e}} \sim 25\,300 - 31\,600 \text{ K}$  (see their Tables 5 and 7, Appendix A here).

Finally, it is of interest to note that the long time-scale of observations of LIN 333 (1984–2009, Table 2) with comparable X-ray and UV fluxes demonstrates a stability of this bright SSS (Mereghetti et al. 2010).

### 3.5. Multiwavelength model SED of CAL 83

As in the case of RX J0513.9-6951, the high values of the near-UV—optical fluxes (a few  $\times 10^{-15} \text{ erg cm}^{-2} \text{ s}^{-1} \text{ \AA}^{-1}$ ), their steepness (e.g.,  $U-B \sim -1 \text{ mag}$ ) and the presence of emission lines of the hydrogen Balmer series, He II  $\lambda 4686$ , N III  $\lambda 4640 \text{ \AA}$  and [O III] 5007  $\text{\AA}$  in the optical spectrum (e.g., Pakull et al. 1985) indicate a strong nebular continuum that dominates the spectrum for  $\lambda > 1\,800 \text{ \AA}$  (see Fig. 1c).

We modeled the SED of CAL 83 between 20.7 and 9000  $\text{\AA}$  by Eq. (2). The best model with *ROSAT* data has the reduced  $\chi^2 = 3.8$  (for 61 d.o.f.) and determines the variables of the SSS,  $\theta_{\text{SSS}} = (6.9 \pm 0.6) \times 10^{-14}$ ,  $T_{\text{BB}} = 345\,000 \pm 15\,000 \text{ K}$  and  $N_{\text{H}} = (1.03 \pm 0.05) \times 10^{21} \text{ cm}^{-2}$ , which yields  $R_{\text{SSS}}^{\text{eff}} = 0.15 \pm 0.02 (d/49 \text{ kpc}) R_{\odot}$  and  $L_{\text{SSS}} = (1.1 \pm 0.5) \times 10^{39} (d/49 \text{ kpc})^2 \text{ erg s}^{-1}$ . Model variables of the nebular component of radiation,  $k_{\text{N}} = (1.0 \pm 0.1) \times 10^{13} \text{ cm}^{-5}$  and  $T_{\text{e}} = 30\,000 + 20\,000 / - 10\,000 \text{ K}$  correspond to  $EM = (2.9 \pm 0.3) \times 10^{60} (d/49 \text{ kpc})^2 \text{ cm}^{-3}$  (Table 3).

The model SED with *Chandra/XMM-Newton* fluxes is very similar to that with the *ROSAT* data (see Fig. 1c, Table 3). The corresponding parameters of the SSS are,  $N_{\text{H}} = (1.3 \pm 0.05) \times 10^{21} \text{ cm}^{-2}$ ,  $T_{\text{BB}} = 357\,000 \pm 15\,000 \text{ K}$ ,  $R_{\text{SSS}}^{\text{eff}} = 0.16 \pm 0.02 (d/49 \text{ kpc}) R_{\odot}$

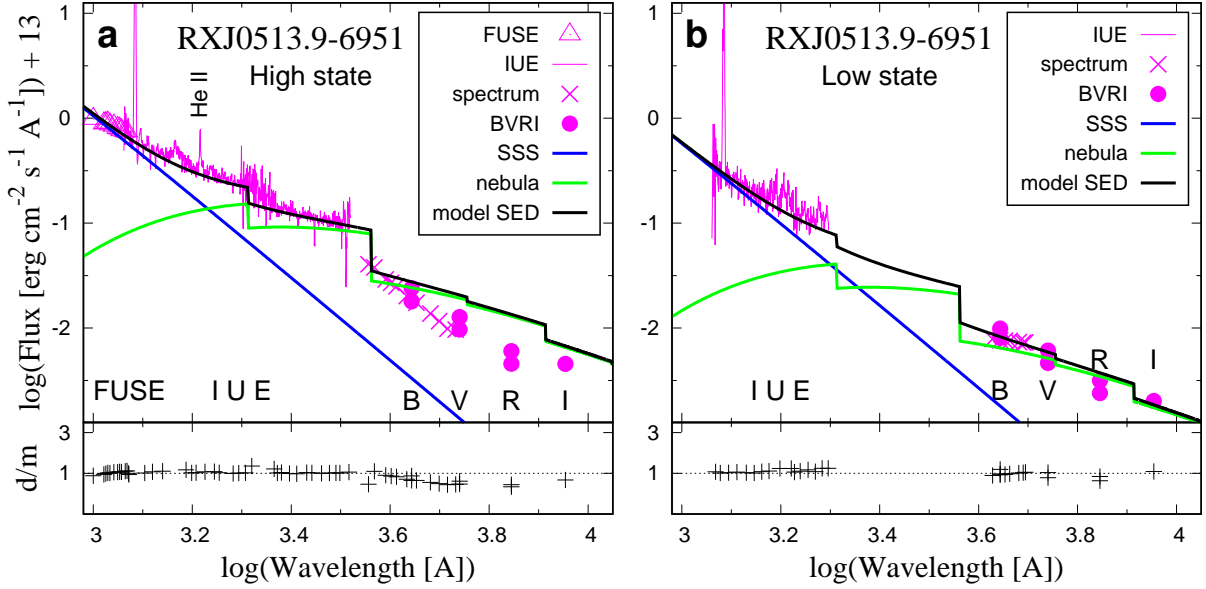


**Figure 2.** The UV–optical SED during the optical-high (a) and low (b) state of RX J0513.9-6951. This demonstrates that the pronounced optical variability with  $\Delta V \approx 1$  mag can be caused by the variable nebular emission (Sect. 3.3).

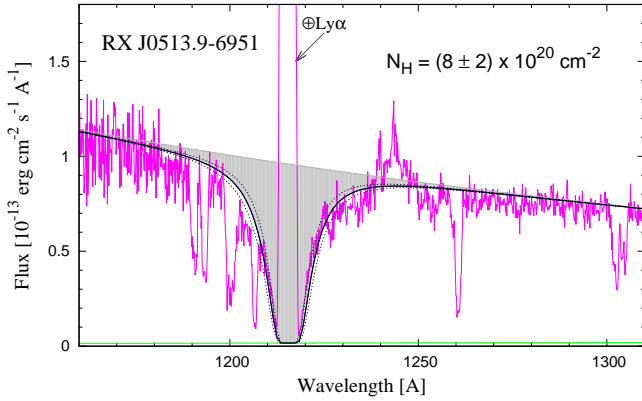


**Figure 3.** The *HST*/*GHRS* spectrum of RX J0513.9-6951 dereddened with  $E_{B-V} = 0.11$  (in magenta). A strong depression of the continuum around the Ly- $\alpha$  line (grey area) is caused by Rayleigh scattering of the SSS radiation on hydrogen atoms with a column density of  $(8 \pm 2) \times 10^{20} \text{ cm}^{-2}$  (black and dotted lines). Meaning of blue and green lines as in Fig. 1. Geocoronal Ly- $\alpha$  line is denoted by  $\oplus$ .

and  $L_{\text{SSS}} = (1.4 \pm 1.1) \times 10^{39} (d/49 \text{ kpc})^2 \text{ erg s}^{-1}$ . As in the case of LIN 333, the long time-scale of observations demonstrate that CAL 83 is a stable SSS during its X-ray-on states.

Finally, the attenuation of the continuum around Ly- $\alpha$ , observed on the *HST*/*GHRS* spectrum, corresponds to  $N_{\text{H}} = (8 \pm 2) \times 10^{20} \text{ cm}^{-2}$  (see Fig. 4).

### 3.6. Multiwavelength model SED of RX J0527.8-6954

The steepness of the SWP45499 spectrum suggests that the SSS radiation dominates also a wide range

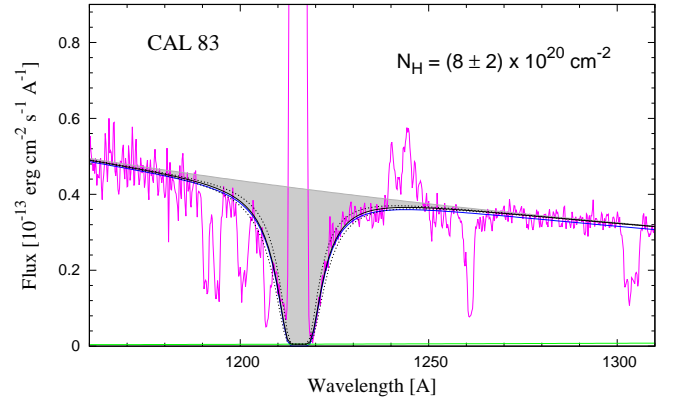


**Figure 4.** As in Fig. 3, but for CAL 83. The spectrum is dereddened with  $E_{B-V} = 0.11$ .

of the far-UV continuum (115–190 nm), while the LWP23826 spectrum has an opposite slope, whose profile suggests a dominant contribution from a low temperature nebula (see Fig. 1d). Available observations allow us to model the continuum fluxes between 26.5 and 5500 Å. The best fit to the X-ray and UV data (39 fluxes) has the reduced  $\chi^2 = 3.3$  (for 34 d.o.f.) and determines the model variables,  $\theta_{\text{SSS}} = (7.3 \pm 0.7) \times 10^{-14}$ ,  $T_{\text{BB}} = 255\,000 \pm 20\,000 \text{ K}$  and  $N_{\text{H}} = (7.1 \pm 0.2) \times 10^{20} \text{ cm}^{-2}$ , which yield  $R_{\text{SSS}}^{\text{eff}} = 0.16 \pm 0.02 (d/49 \text{ kpc}) R_{\odot}$  and  $L_{\text{SSS}} = (3.7 \pm 0.5) \times 10^{38} (d/49 \text{ kpc})^2 \text{ erg s}^{-1}$ . The nebular component of radiation is determined by  $k_{\text{N}} = (1.5 \pm 0.1) \times 10^{13} \text{ cm}^{-5}$  and  $T_{\text{e}} = 9\,000 \pm 2\,000 \text{ K}$  that gives  $EM = (4.3 \pm 0.3) \times 10^{60} (d/49 \text{ kpc})^2 \text{ cm}^{-3}$  (Table 3).

## 4. DISCUSSION

#### 4.1. Amount of absorption to the SSSs

Independently of the SED modeling, we estimated the value of  $N_{\text{H}}$  also from Rayleigh scattering of the SSS radiation on H atoms that creates a strong depression of the continuum around the Ly $\alpha$  line (see Figs. 3 and 4). The larger inaccuracy of this method is given by a weaker sensitivity of the Rayleigh scattering process to the amount of scatterers in the Ly $\alpha$  wings, and by the complexity of the depression profile due to superposition of rich absorption-line spectrum to the continuum. On the other hand, determination of  $N_{\text{H}}$  from the SED modeling suffer by rather uncertain X-ray fluxes taken from already published figures and their extreme sensitivity to the amount of absorption within the supersoft X-ray wavelengths. Another source of uncertainties in determining values of  $N_{\text{H}}$  is given by using non-simultaneous X-ray and UV observations, the temporal variability of the SSS radiation, and/or the circumstellar component of  $N_{\text{H}}$  originating in the surrounding nebula (Sect. 4.6, Appendix A). Nevertheless,  $N_{\text{H}}$  values obtained by these two different methods are comparable (see Table 3, and Figs. 3 and 4 for RX J0513.9-6951 and CAL 83). In the case of LIN 333 and CAL 83 we modeled different X-ray data together with the same UV–optical observations (Table 3, Figs. 1b and 1c). Despite this shortcoming, the  $N_{\text{H}}$  values we found for LIN 333 are in good agreement with the total column density  $N_{\text{H}} \approx (7 \pm 4) \times 10^{20} \text{ cm}^{-2}$  determined by Wang (1991), which includes contributions in the Galaxy, in the SMC, and inside the nebula. For RXJ0527.8-6954 we used X-ray fluxes from June 1990 and probably fainter far-UV fluxes from September 1992 as suggested by the X-ray and optical light curves (see Greiner et al. 1996; Alcock et al. 1997). If this is so, the true value of  $N_{\text{H}}$  should be little higher than that given in Table 3.

#### 4.2. Comparison with previous models

Figure 5 compares our multiwavelength models and the X-ray-data models from the literature described in Sects. 1.1 to 1.4, and summarized in Table 1. In both cases, the SED models match satisfactorily the absorbed X-ray fluxes. However, the unabsorbed models differ, often significantly, from our multiwavelength models. Mostly, they are a factor of  $\sim 10 - 100$  below the far-UV data. Such the discrepancy between the multiwavelength modeling and the modeling only the X-ray data can be ascribed to the mutual dependence between  $N_{\text{H}}$ ,  $L_{\text{SSS}}$ , and  $T_{\text{BB}}$  parameters, as described in Sect. 4.1 of Skopal (2015).

RX J0513.9-6951: The X-ray blackbody solution of Schaeidt et al. (1993) corresponds to  $L_{\text{SSS}} = 2.3 \times 10^{38} \text{ erg s}^{-1}$ , which is a factor of  $\sim 15$  below the far-

UV fluxes. The model atmosphere fit by Gänsicke et al. (1998) yields even lower luminosity of  $(2.5 - 9) \times 10^{37} \text{ erg s}^{-1}$  (see Sect. 1.1).

RX J0058.6-7135 (LIN 333): Blackbody and atmospheric X-ray SED models performed by Heise et al. (1994) are a factor of  $\sim 9$  and  $\sim 300$  below the *FUSE* data, respectively. They were already discussed by Skopal (2015) as an illustrative example of the mutual dependence of the model parameters,  $N_{\text{H}}$ ,  $L_{\text{SSS}}$  and  $T_{\text{BB}}$  (see Sect. 4.1 and Fig. 7 there). Similar results were obtained also by Mereghetti et al. (2010) using the *XMM-Newton* observations (see Table 1). The authors questioned their atmospheric model when they found that the flux predicted in the visible band is lower by  $\sim 30\%$  than the upper limit ( $V \sim 21$ ) obtained from the *HST* imaging of the central star by Villaver et al. (2004).

RX J0543.6-6822 (CAL 83): Blackbody solution at the Eddington limit ( $N_{\text{H}} = 8 \times 10^{20} \text{ cm}^{-2}$ ,  $kT_{\text{BB}} = 43 \text{ eV}$ ,  $R_{\text{BB}} = 1.5 \times 10^9 \text{ cm}$ , Greiner et al. 1991) is a factor of  $\sim 20$  below the far-UV continuum, while their softer model ( $N_{\text{H}} = 1.7 \times 10^{21} \text{ cm}^{-2}$ ,  $kT_{\text{BB}} = 26 \text{ eV}$ ) fits the absorbed X-ray data for  $\theta_{\text{SSS}} \sim 4 \times 10^{-13}$  (i.e.,  $R_{\text{BB}} = 6.0 \times 10^{10} \text{ cm}$ ,  $L_{\text{SSS}} \sim 2 \times 10^{40} \text{ erg s}^{-1}$ ) that is a factor of  $\sim 30$  above the far-UV fluxes. Independent modeling of the *BeppoSAX* spectrum of CAL 83 by Parmar et al. (1998) also matches well the observed X-ray data, but the unabsorbed model is by a factor of  $\sim 80$  below the far-UV continuum.

RX J0527.8-6954: Similar results were obtained also for this SSS by Greiner et al. (1991).

Figure 6 compares our SED model for RX J0513.9-6951 and that of Popham & di Stefano (1996), who calculated models of irradiated flared accretion disks around luminous steady-burning WDs in bright LMC SSSs (CAL 83, CAL 87, and RX J0513.9-6951) and compared the resulting disk fluxes to optical and UV observations. To increase the radiation from the disk at these wavelengths, the disk has to be flared to reprocess sufficiently large amount (more than 1/4) of the WD radiation into the optical and UV (see their Fig. 2). Figure 6 shows their resulting model (gray line) that consists of three components of radiation: (i) From a  $1.2 M_{\odot}$  steady-burning WD ( $\dot{M}_{\text{acc}} = 5 \times 10^{-7} M_{\odot} \text{ yr}^{-1}$ ,  $L_{\text{WD}} = 1.5 \times 10^{38} \text{ erg s}^{-1}$ ,  $T_{\text{BB}} = 5 \times 10^5 \text{ K}$  and  $R_{\text{WD}} = 1.84 \times 10^9 \text{ cm}$ ), (ii) from the irradiated disk, whose heated surface increases the optical and UV fluxes by a factor of 3–5, while the heated star-disk boundary makes much brighter the high-energy spectrum, and (iii) from the irradiated fraction of the donor star that contributes mainly in the optical spectrum. For a comparison, the disk spectrum with no external heating corresponding to the above-mentioned parameters (i.e., the accretion

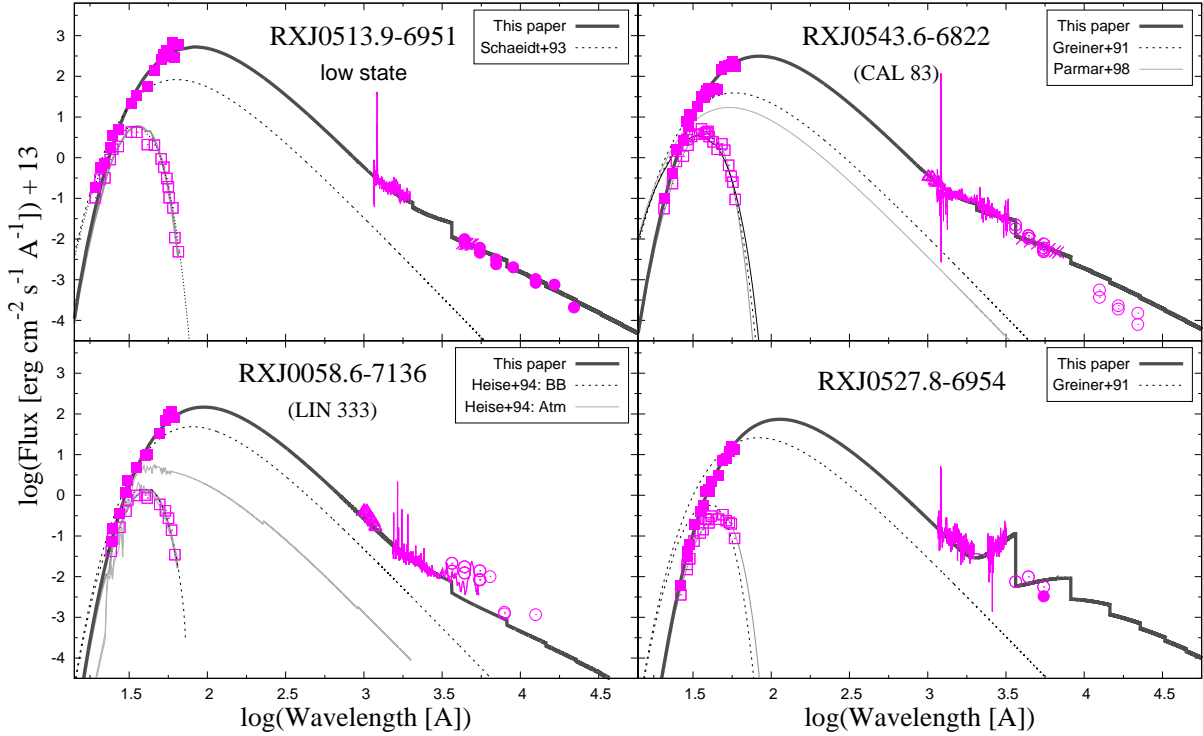


**Figure 5.** Comparison of the multiwavelength SED models of this paper (dark thick lines, Table 3) and the corresponding X-ray-data blackbody models from the literature (see legends, Table 1, Sect. 4.2).

luminosity of  $2.7 \times 10^{36} \text{ erg s}^{-1}$ ) and the outer disk edge of  $1.35 \times 10^{11} \text{ cm}$  (Popham & di Stefano 1996) is shown by the dashed line<sup>2</sup>. Note that a more sophisticated calculation performed by Popham & di Stefano (1996) provides similar profile of the disk spectrum, but it is just somewhat shifted to shorter wavelengths (see their Figs. 1 and 2). The Popham & Di Stefano’s model is calculated for the disk inclination of  $60^\circ$ . If viewing the disk face-on, its flux increases twice, and will match better the measured UV and optical fluxes. However, it is rather below the NIR fluxes and does not reproduce their slope. The model does not match the X-ray fluxes, at all.

Our multiwavelength SED models of the bright SSSs correspond to super-Eddington luminosity even for a high-mass WD accretor. The SED from the near-UV to longer wavelengths indicates a dominant contribution from thermal nebula. Both results are fairly startling with respect to the present picture of SSSs, whose luminosities can reach in maximum the Eddington limit for a WD accretor, and the UV–optical spectrum is thought to be dominated by the light from accretion disk irradiated by the central steady-burning WD

<sup>2</sup> For the sake of simplicity, we adopted optically thick disk that radiates locally like a blackbody (Warner 1995).

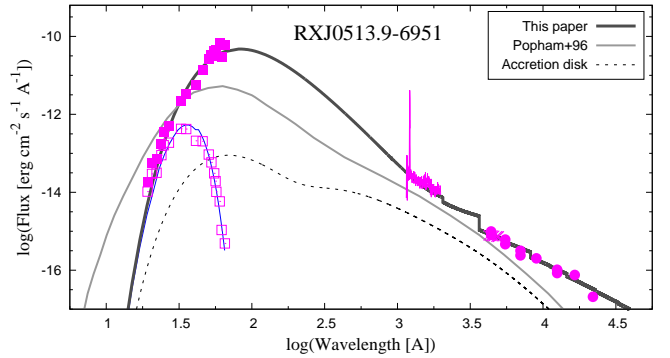


**Figure 6.** Comparison of our SED model for RX J0513.9-6951 and that including the steady-burning WD at the Eddington limit irradiating the flared accretion disk and the donor star (gray line, adopted from Fig. 4 of Popham & di Stefano 1996). The model is aimed to explain the strong UV and optical fluxes. Compared is a spectrum of accretion disk with no external heating (dashed line, Sect. 4.2).

(Popham & di Stefano 1996). Below, we discuss these properties in detail.

### 4.3. Problem of the high luminosity

#### 4.3.1. Accreting white dwarf ?

According to van den Heuvel et al. (1992), the radiation of SSSs is generated by a stable nuclear burning of

hydrogen accreted onto massive WDs. This idea is based on a theoretical conclusion that there is a small range of accretion rates,  $\dot{M}_{\text{acc}}$ , at which the hydrogen-rich material is quasi-steady burning on the WD's surface as it is accreting (Paczynski & Zytkov 1978; Fujimoto 1982). The material is transported onto the accretor through an accretion disk. Then, the maximum luminosity of a SSS is given by that generated by the nuclear burning on the WD surface and the gravitational potential energy of the accretor, converted into the radiation by the disk and its boundary layer, i.e.,

$$L_{\text{SSS}} = \eta X \dot{M}_{\text{acc}} + \frac{GM_{\text{WD}} \dot{M}_{\text{acc}}}{R_{\text{WD}}}, \quad (5)$$

where  $\eta \sim 0.007 \times c^2 \sim 6.3 \times 10^{18} \text{ erg g}^{-1}$  is the energy production of 1 gram of hydrogen due to the nuclear fusion of 4 protons, and  $X \equiv 0.7$  is the hydrogen mass fraction in the accreted matter.  $M_{\text{WD}}$  and  $R_{\text{WD}}$  are the WD mass and radius. However, even the extreme parameters of the WD accretor,  $M_{\text{WD}} \sim 1.4 M_{\odot}$ ,  $R_{\text{WD}} \sim 0.003 R_{\odot}$  (Panei et al. 2000) and the mass transferred through the disk at a high rate of a few times  $10^{-7} M_{\odot} \text{ yr}^{-1}$  that sustains the stable H-burning (see e.g., Fig. 2 of Shen & Bildsten 2007) generates the total luminosity of  $\gtrsim 10^{38} \text{ erg s}^{-1}$ , which is one order of magnitude below that suggested by our multiwavelength models SED (Table 3). The observed luminosity would require a high accretion rate of  $\dot{M}_{\text{acc}} \sim 10 \dot{M}_{\text{Edd}}$ , where  $\dot{M}_{\text{Edd}}$  is the Eddington accretion rate. This result is not consistent with the model of steady burning WD for the brightest SSSs in LMC and SMC, unless the radiation of the source is not isotropic. Here, the emission from steady nuclear burning onto a WD should be beamed with a factor,  $L/L_{\text{sph}} \lesssim 0.1$ , where  $L_{\text{sph}}$  is the inferred isotropic luminosity and  $L$  is the true source luminosity.

#### 4.3.2. Accreting neutron star ?

A neutron star (NS) as the accretor in the brightest SSSs provides a somewhat better possibility to explain their high luminosities, because of a larger efficiency in converting gravitational energy into the heat and radiation. The efficiency of radiative emission in units of the total mass energy accreted on a compact object is

$$\xi = \frac{L_{\text{SSS}}}{\dot{M}_{\text{acc}} c^2} = \frac{GM_{\text{acc}}}{R_{\text{acc}} c^2}. \quad (6)$$

For a  $1.4 M_{\odot}$  NS with a radius of 10–15 km,  $\xi \sim 0.2 - 0.14$ , while for a WD ( $1 M_{\odot}$ , 7000 km),  $\xi \sim 2 \times 10^{-4}$ . Considering that the efficiency of turning mass energy into radiation via the nuclear fusion is of  $\sim 7 \times 10^{-3}$  (Eq. (5)), the nuclear fusion reactions can be a vital source of energy for accreting WDs, but are negligible in converting the mass energy accreted by a NS.

To generate the luminosity of  $\sim 10^{39} \text{ erg s}^{-1}$ , the above mentioned parameters of a NS require the accretion rate  $\dot{M}_{\text{acc}} = 0.85 - 1.3 \times 10^{-7} M_{\odot} \text{ yr}^{-1}$ . These values are more realistic than those required by the WD accretor. Such the material can be supplied by mass transfer from a close Roche-lobe filling companion. However, these accretion rates are still above the critical values even for a high mass NS.

The presence of a NS as the accretor in the luminous SSSs could be evidenced by e.g., detection of strictly periodic short-term light variation on the time-scale of milliseconds to seconds, or by direct measuring of the size of the X-ray emission region from eclipse analysis (Mukai 2017). However, no such observations indicating these properties of SSSs have been reported yet. In the cases, where a NS probably accretes from the wind of its companion, we measure a significantly harder X-ray spectrum dominating 1–10 keV (Masetti et al. 2007b,a) than it is generated by our brightest SSSs. Therefore, the presence of accreting NSs in the brightest LMC and SMC SSSs seems unlikely.

#### 4.3.3. Accreting black hole ?

The high X-ray luminosities  $L_{\text{X}} \gtrsim 10^{39} \text{ erg s}^{-1}$  can be interpreted by a sub-Eddington accretion onto intermediate-mass black hole (BH, Freeland et al. 2006). For example, Kong & Di Stefano (2003) applied this possibility to the luminous SSS XMMU J005510.7–373855 in the spiral galaxy NGC 300 ( $L_{\text{bol}} = 0.2 - 2 \times 10^{39} \text{ erg s}^{-1}$ ), and found that accretion disk around a  $\approx 2800 M_{\odot}$  BH radiating at  $kT = 60 \text{ eV}$  is required to generate the luminosity of  $10^{39} \text{ erg s}^{-1}$ . However, such the massive BHs, that are usually connected with the star-forming regions (Irwin et al. 2004), are unlikely to be present in LMC and SMC.

On the other hand, King (2008) considered that the high luminosity of ultraluminous X-ray sources (ULXs) is generated by a stellar-mass BH accreting material from a close companion star at super-Eddington rates ( $\dot{M}_{\text{acc}} > \dot{M}_{\text{Edd}}$ ) with some degree of geometric beaming. According to Gladstone et al. (2009), a relatively cool SSS photosphere for the super-Eddington accretion flows could be created by a massive wind that completely envelopes the inner-disc regions. They also concluded that all spectral features in their sample of ULXs can be explained by stellar mass BHs at high accretion rates.

However, there are two main observational arguments contradicting the presence of BHs in the brightest SSSs in LMC and SMC.

- First, it is the profile of the X-ray spectrum that is considerably harder than that produced by our brightest SSSs (Jin et al. 2010; Soria & Kong

2016). In addition, the spectral shape of ULXs can show either a single peak at 2-3 keV or two peaks (one below 1 keV and one above 3 keV, see Gladstone et al. 2009), or otherwise structured shape of the spectrum (Motch et al. 2014; Urquhart & Soria 2016) – all totally different from those, here studied, brightest SSSs.

- Second, if the jets are observed, their velocities are expected to be comparable to the escape velocity of the central compact object (Livio 1997). Accordingly, jets observed from objects containing a BH accretor are accelerated to relativistic speed (Mirabel & Rodríguez 1999; Fender et al. 2006; Takeuchi et al. 2010; Liu et al. 2015), while those launched by a WD accretor reach speeds of the order of thousands of  $\text{km s}^{-1}$  only (Southwell et al. 1996; Becker et al. 1998; Skopal et al. 2009b).

Therefore, considering the observed X-ray SEDs of our targets, and taking into account that jets from RX J0513.9-6951 are ejected at  $\pm 3800 \text{ km s}^{-1}$  (Southwell et al. 1996), there is no other option than that a WD is present also in the most luminous SSSs in LMC and SMC.

#### 4.3.4. Luminous post-nova supersoft X-ray sources ?

Due to the above reasons, we assume that the accretor in the brightest SSSs, we investigate in this paper, is a WD. A possibility how to keep a SSS at the super-Eddington state for a long time is to fuel the burning WD after the classical nova eruption, when it is in the post-nova SSS state, and is burning at/above the nuclear Eddington limit, i.e., producing the super-Eddington luminosity. Below we support this idea by observations of similar cases, and theoretical considerations.

**Examples from observations.** A transient post-nova SSS phase occurs after the optical outburst and is of varying duration. The shortest one is measured for the 1 yr recurrent nova M31N 2008-12a in the Andromeda galaxy that lasts for about two weeks (Henze et al. 2018), while in the cases of GQ Mus and LMC 1995, the SSS phase was detected for  $\sim 10$  yr (Oegelman et al. 1993; Shanley et al. 1995) and 6–8 yr (Orio et al. 2003), respectively. Long-lasting super-Eddington luminosity was also documented for some extraordinary novae, e.g., FH Ser (Friedjung 1987), LMC 1988 #1 (Schwarz et al. 1998), LMC 1991 (Schwarz et al. 2001), SMCN 2016-10a (Aydi et al. 2018), and nova V339 Del (Skopal 2019). The unusually long phase of hydrogen burning was indicated for the nova V723 Cas (1995) by detecting it as a bright SSS more than 12 years after the outburst, with possible super-Eddington luminosity (depending on the spectral model, see Ness et al.

2008). The transient SSS in the nearby galaxy NGC 300, denoted as SSS<sub>1</sub>, has the bolometric luminosity of  $\approx 10^{39} \text{ erg s}^{-1}$  (Kong & Di Stefano 2003). The source was found in outburst in 1992, 2000, 2008 and 2016 suggesting a possible recurrence period of about 8 years, and thus could be associated with a recurrent nova (Carpano et al. 2019). Recently, Vasilopoulos et al. (2020) discovered a 30-yr long-lived post-nova SSS in LMC undergoing residual surface nuclear burning. A large number of post-nova SSSs (250–600) was identified in M31 (Soraisam et al. 2016). The authors found that depending on the WD mass distribution in novae, their unabsorbed X-ray luminosity distribution shows significant steepening around  $L_X(0.2 - 1.0 \text{ keV}) \approx 10^{38} \text{ erg s}^{-1}$  with a maximum at  $\approx 2 \times 10^{38} \text{ erg s}^{-1}$ . According to our multiwavelength SED modeling,  $L_{\text{SSS}}/L_X(0.2 - 1.0 \text{ keV}) \gtrsim 10$  (see Table 3), which would correspond to the bolometric luminosities of the brightest SSSs in M31 of  $\approx 10^{39} \text{ erg s}^{-1}$ . Note, however, that this ratio is a strong function of the temperature:  $L_{\text{SSS}}/L_X(0.2 - 1.0 \text{ keV}) \sim 21$  or  $\sim 2.4$  only for 300 000 or 600 000 K, respectively. Finally, long-term accretion at/above the nuclear Eddington limit is also indicated for symbiotic X-ray binaries RXJ0059.1-7505 (LIN 358) in SMC (Skopal 2015; Kuuttilla et al. 2021; Washington et al. 2021) and Draco C1 in the Draco dwarf spheroidal galaxy (Saeedi et al. 2018; Lewis et al. 2020), where the donor star is an evolved red giant.

**Theoretical considerations.** According to Kovetz et al. (1988) the irradiation of the donor star after the nova outburst can cause the red dwarf to expand and induce a mass transfer rate enhanced by two orders of magnitude. If the donor is a red giant (symbiotic binaries), the high wind-mass-transfer efficiency is achieved by the wind focusing to the orbital plane (Skopal & Cariková 2015; Shagatova et al. 2016, 2021). In this case, the enhanced accretion can be sustained also through the disk warping that leads to ejection of transient jets (Skopal et al. 2018). If the accretion resumes immediately at the beginning of the post-nova SSS phase, the SSS lifetime can be substantially lengthened (Kato et al. 2017). Illustration of this effect is in Fig. 15 of Henze et al. (2018). At a high accretion rates ( $\gtrsim 5 \times 10^{-7} M_{\odot} \text{ yr}^{-1}$ ), so that a new outburst can occur on the human lifetime, the SSS phase can be interrupted for a relatively short time by the optical outburst being followed by the SSS phase at very high bolometric luminosity. Such the type of variability has been observed for the SSS SSS<sub>1</sub> in NGC 300 (see above), and here for RX J0527.8-6954, where the repeatability of its visibility is indicated on the timescale of  $\approx 20$  years (Sect. 1.4).

According to the above-mentioned reasons we suggest that the brightest SSSs could be unidentified optical novae that are in a post-nova SSS state, when the residual surface nuclear burning is supported by rapid re-accretion from the donor, which can help in sustaining the high luminosity of the burning WD for a long time. The lifetime of the high luminosity, possibly super-Eddington, will then depend on the energy output from both the residual burning and the resumed accretion.

#### 4.4. Mass-loss rate from the nebular emission

The high luminosities of SSSs, whose WDs probably accrete at a high rate, lead to a mass-outflow in the form of a wind (e.g., Kato & Hachisu 1994; Hachisu & Kato 2001, and Appendix A here). According to Kato & Hachisu (1994) the optically thick/thin interface of the wind represents the SSS pseudo-photosphere. In our cases, its average value is  $R_{\text{SSS}}^{\text{eff}} \sim 0.17 R_{\odot}$  (Table 3). The optically thin wind above the hot and luminous pseudo-photosphere is ionized, giving rise to the nebular radiation (see Appendix A). Assuming that the wind flows out spherically symmetrically at a constant velocity  $v_{\infty}$ , begins at the  $R_{\text{SSS}}^{\text{eff}}$ , and its radial density distribution satisfies the mass continuity equation, then the relationship between the mass-loss rate of the ionized wind,  $\dot{M}_{\text{SSS}}$ , and its emission measure,  $EM$ , can be expressed as,

$$\dot{M}_{\text{SSS}} = [4\pi (\mu m_{\text{H}} v_{\infty})^2 R_{\text{SSS}}^{\text{eff}} EM]^{1/2} \text{gs}^{-1}, \quad (7)$$

(see Eq. (7) of Skopal et al. 2014), where  $\mu$  is the mean molecular weight and  $m_{\text{H}}$  is the mass of the hydrogen atom. This relation assumes that the outer radius of the ionized wind  $\gg R_{\text{SSS}}^{\text{eff}}$ . The average value of  $R_{\text{SSS}}^{\text{eff}} = 0.17 R_{\odot}$  and  $EM \gtrsim 10^{60} \text{cm}^{-3}$  (Table 3) yield  $\dot{M}_{\text{SSS}} \gtrsim 2 \times 10^{-6} M_{\odot} \text{yr}^{-1}$  for  $v_{\infty} \equiv 1000 \text{km s}^{-1}$ .

Using the same assumptions as for the nebular continuum, similar values of  $\dot{M}_{\text{SSS}}$  can be obtained also from hydrogen emission lines, because they are formed in the same volume of the ionized hydrogen as the continuum. For example, for the measured flux in the  $\text{H}\beta$  line,  $F_{\text{H}\beta}$ , we can express its luminosity as,

$$L_{\text{H}\beta} = 4\pi d^2 F_{\text{H}\beta} = h\nu_{\beta} \alpha(\text{H}\beta, T_e) \int_{R_{\text{SSS}}^{\text{eff}}}^{\infty} n_e(r) n_p(r) dV, \quad (8)$$

where  $\alpha(\text{H}\beta, T_e)$  is the effective recombination coefficient for the  $\text{H}\beta$  transition, and  $n_e$  and  $n_p$  is the concentration of electrons and protons in the spherical  $\text{H}^+$  zone with the inner radius  $R_{\text{SSS}}^{\text{eff}}$ , from which the wind can become optically thin in the  $\text{H}\beta$  line. The integral in Eq. (8) represents the emission measure of the  $\text{H}^+$

region (see Sect. 3.1). Using its expression from Eq. (7), we obtain,

$$\dot{M}_{\text{SSS}} = \left[ 4\pi (\mu m_{\text{H}} v_{\infty})^2 R_{\text{SSS}}^{\text{eff}} \frac{L_{\text{H}\beta}}{h\nu_{\beta} \alpha(\text{H}\beta, T_e)} \right]^{1/2} \text{gs}^{-1}, \quad (9)$$

which corresponds to a lower limit of  $\dot{M}_{\text{SSS}}$ , because in a line transition the wind becomes optically thin above the photosphere, at distances  $> R_{\text{SSS}}^{\text{eff}}$ . This problem was treated by Leitherer (1988), who found that stellar winds of luminous hot stars become optically thin in the  $\text{H}\alpha$  line from a distance of  $\sim 1.5$  times the star's radius. Accordingly,  $F_{\text{H}\beta} = 1.45 \times 10^{-13} \text{erg cm}^{-2} \text{s}^{-1}$  measured in the spectrum of LIN 333 by Aller et al. (1987) corresponds to  $\dot{M}_{\text{SSS}} \sim 1.7 \times 10^{-6} M_{\odot} \text{yr}^{-1}$  for  $\alpha(\text{H}\beta, 30000) = 1.088 \times 10^{-14} \text{cm}^3 \text{s}^{-1}$  (Hummer & Storey 1987),  $R_{\text{SSS}}^{\text{eff}} = 0.17 R_{\odot}$  and  $v_{\infty} \equiv 1000 \text{km s}^{-1}$ . These observational values of  $\dot{M}_{\text{SSS}}$  are also consistent with those suggested by the optically thick wind theory, for winds from the nuclear-burning WDs of a high mass (see Eq. (23) of Kato & Hachisu 1994). It is of interest to note that wind mass-loss rate of the order of  $10^{-6} M_{\odot} \text{yr}^{-1}$  was measured during the long-lasting SSS-phase of the classical nova V339 Del, whose bolometric luminosity was kept at a high level of  $1 - 2 \times 10^{39} \text{erg s}^{-1}$  for  $\sim 150$  days (see Fig. 12 of Skopal 2019).

#### 4.5. Dense unresolved circumstellar nebulae in SSSs

According to the mass continuity equation the particle density of the wind  $n(r) \propto r^{-2}$ , where  $r$  is the radial distance from the source of the wind. For example,  $n(1 R_{\odot}) \sim 9 \times 10^{12} \text{cm}^{-3}$ , while  $n(1 \text{AU}) \sim 2 \times 10^8 \text{cm}^{-3}$  for wind parameters given in Sect. 4.4. Further, the emitted flux by the wind at the distance  $r$  is proportional to  $n^2$  (e.g., Eq. (8)), so the densities in our example correspond to the flux ratio of the wind layers,  $F(1 \text{AU})/F(1 R_{\odot}) = 4\pi(1 \text{AU})^2 n(1 \text{AU})^2 / 4\pi(1 R_{\odot})^2 n(1 R_{\odot})^2 \sim 2 \times 10^{-5}$ . This implies that the vast majority of the nebular emission is produced within a relatively small central part of the ionized wind – from its optically thick/thin interface up to a few AU. Such dimensions of nebular medium are similar to those generated by accreting nuclear-burning WDs in symbiotic stars (Skopal 2005), and were also considered by Nielsen & Gilfanov (2015) in calculations the circumstellar mass-loss rates required for obscuration of supersoft X-ray sources. For the purpose of our work, it is important to note that such a small size of the circumstellar nebulae in SSSs at the distance of LMC and SMC is not spatially resolvable by the current observational technique. Further, the circumstellar nebulae generated by the ionized wind in a binary are also

very dense. In our cases, the emission measure ( $\sim n^2V$ ) of a few times  $10^{60} \text{ cm}^{-3}$  (Table 3) corresponds to the mean particle density of a few times  $10^9 \text{ cm}^{-3}$ . Such the dense nebulae are characterized with a specific type of the emission line spectrum, whose fluxes and their theoretical ratios significantly differ from those produced by the low-density planetary nebulae and/or ISM nebulae predicted to be photoionized by the central SSS (see suggestions for future work in Sect. 5). Here, for a comparison with a dense circumstellar nebula in the symbiotic star AX Per, Skopal et al. (2001) found the electron concentration in the H II and [O III] zone surrounding its burning WD to be of a few times  $10^9$  and  $\approx 3 \times 10^7 \text{ cm}^{-3}$ , respectively. Further, they suggested that the extremely steep Balmer decrement (e.g.,  $H\alpha/H\beta \sim 7 - 10$ ) could be due to electron collisions in a very dense H II region.

Finally, we note that the dense unresolvable circumstellar nebulae can be indicated for a given object only by the method of disentangling its composite spectrum (Sect. 3.1).

#### 4.6. Origin of the X-ray/optical flux anticorrelation

The presence of a strong nebular radiation in the UV to NIR spectrum of our targets ( $EM \gtrsim 2 \times 10^{60} \text{ cm}^{-3}$ , Table 3) and its variation (Fig. 2, Sect. 3.3) allow us to explain the anticorrelation between their supersoft X-ray and optical fluxes by a variable mass-outflow from the accreting burning WD as in the case of the symbiotic binary AG Dra (see González-Riestra et al. 2008; Skopal et al. 2009a). It is assumed that the variable mass-outflow results from a variable mass-transfer. Charles et al. (2010) suggested a similar view for the SSS RX J0513.9-6951, and also estimated the mass outflow rate of  $\approx 10^{-7} M_{\odot} \text{ yr}^{-1}$  for the luminosity at the Eddington limit.

An increase of the mass-loss increases the particle density above the hot WD's pseudo-photosphere, and thus the number of b-f absorptions. This leads to a *decrease* of the supersoft X-ray photons, and consequently to an increase of f-b and f-f transitions that causes an *increase* of the nebular emission, which dominates the spectrum from the near-UV to longer wavelengths.

In this way the enhanced (wind) mass-outflow increases the optical depth for the supersoft X-ray photons, and thus increases its optically thick/thin interface, which is the WD's pseudo-photosphere. That is why we indicate a larger effective radius of the SSS during the X-ray-off/optical-high states. For RX J0513.9-6951 the  $R_{\text{SSS}}^{\text{eff}}$  radius inflated from  $\sim 0.19 R_{\odot}$  during the optical-low state to  $\sim 0.26 R_{\odot}$  during the optical-high state (Sect. 3.3, Table 3). Independently, the connection between the flux anticorrelation and the WD's radius

was demonstrated for RX J0513.9-6951 by Charles et al. (2010) on the basis of the XMM-Newton simultaneous soft X-ray, UV and optical observations (see their Figs. 2 and 3). Finally, the inflated WD can also increase its radiation for  $\lambda > 912 \text{ \AA}$  (compare the blue lines in the panel **a** and **b** of Fig. 2).

In this way, the ionization/recombination process in the *variable* wind from the SSS causes the simultaneous presence of the X-ray-on/off and optical-low/high states. Corresponding changes in the nebular emission can explain  $\sim 1$  mag changes in the optical brightness (Sect. 3.3).

## 5. CONCLUSIONS AND FUTURE WORK

In this paper we performed the multiwavelength modeling of the supersoft X-ray—NIR SED for the brightest Magellanic Cloud SSSs, RX J0513.9-6951, RX J0543.6-6822, RX J0058.6-7135 and RX J0527.8-6954. The global SED models satisfactorily fit the measured multi-band fluxes. The main results of the modeling can be summarized as follows.

1. The SED models revealed that their fundamental parameters,  $L_{\text{SSS}}$ ,  $T_{\text{BB}}$  and  $R_{\text{SSS}}^{\text{eff}}$  are  $\gtrsim 10^{38} - 10^{39} \text{ erg s}^{-1}$ ,  $\approx 3 \times 10^5 \text{ K}$  and  $\sim 0.17 R_{\odot}$ , respectively. Their supersoft radiation is attenuated with the total  $N_{\text{H}} \sim (7 - 12) \times 10^{20} \text{ cm}^{-2}$ . The modeling identified the nebular component of radiation with  $EM \gtrsim 2 \times 10^{60} \text{ cm}^{-3}$  (Table 3). Luminosities of our targets differ significantly from those inferred previously from modeling the X-ray data only (Sect. 4.2, Fig. 5).
2. In spite of super-Eddington luminosities for a  $1.4 M_{\odot}$  compact object, the accretor has to be a WD, because the X-ray spectrum profile and a low speed of jets are not consistent with those of accreting NS or BH (Sects. 4.3.2 and 4.3.3).
3. The high luminosities lead to the mass-loss at high rates. Assuming that the nebular component of radiation is produced by the ionized wind from SSSs, its emission measure corresponds to the mass-loss rate  $\gtrsim 2 \times 10^{-6} M_{\odot} \text{ yr}^{-1}$  (Sect. 4.4). The ionized wind represents a dense unresolved circumstellar nebula in SSSs (Sect. 4.5, Appendix A).
4. Accordingly, we suggest that the brightest SSSs in LMC and SMC could be unidentified optical novae in a post-nova SSS state, whose lifetime and luminosity are enhanced by the resumed accretion, possibly at super-Eddington rates (Sect. 4.3.4).
5. The observed anticorrelation between the supersoft X-ray and optical fluxes can be caused by a

variable mass-outflow from the SSS due to variations in the mass-transfer. A higher mass-loss absorbs more X-ray photons that are re-emitted in the form of the nebular emission, and vice versa. As a result, we observe simultaneously the X-ray-off/on and optical-high/low states (Sect. 4.6).

For future investigation, we suggest to use the multi-wavelength modeling including simultaneously obtained fluxes from both ascending and descending part of the SSS spectrum. In this way to determine more reliable parameters than can be obtained by modeling only one part of the spectrum. To test the proposed model, and develop its more perfect version we suggest to acquire new observations, and using better theoretical modeling. In particular the following.

- Flux calibrated low-resolution optical/NIR spectrum ( $\lambda \gtrsim 350\text{nm}$ ) should verify the presence of the nebular continuum in the spectrum by its specific profile and the presence of the Balmer jump in emission. Moreover, for LIN 333, such the spectrum should confirm or refute its binary nature proposed in Appendix C.
- High-resolution spectra should directly indicate a high-velocity mass-outflow by (presumably) broad wings of the strongest lines as  $H\alpha$ ,  $H\beta$  and  $\text{He II } \lambda 4686$ . In addition, for RX J0513.9-6951, the presence of satellite components to these lines would indicate a collimated bipolar outflow resulting from a very high accretion rate onto the WD (see Southwell et al. 1996).
- In accordance with the study of Nielsen & Gilfanov (2015), using the photoionization code CLOUDY, determine the critical value of the mass-loss rate,  $\dot{M}_{\text{crit}}$ , from the burning WD that causes the obscuration of the central X-ray source for parameters determined by our modeling. The corresponding  $EM$  should be comparable with that obtained from the SED modeling during the X-ray-off states. In this way to test the origin of the X-ray/optical flux anticorrelation by a variable wind from the SSS proposed in Sect. 4.6. Furthermore, the calculated emission line spectrum produced by the ionized wind from the X-ray source should provide additional constraints on the SSS environment. By analogy with symbiotic stars, a dense (unresolved) nebula, here suggested also for SSSs by our SED modeling (Sect. 4.5; Appendix A), should be characterized by an anomalous Balmer decrement (e.g.,  $H\alpha/H\beta \gg 3$ ), and a very low rate of the nebular  $[\text{O III}]$  lines to

$[\text{O III}] \lambda 4363$  – in strong contrast to values produced by the low-density planetary nebulae (e.g., Gurzadyan 1997), and/or nebulae predicted to exist around SSSs imbedded in the low-density ISM (Nielsen & Gilfanov 2015, Sect. 4.5 here).

- In modeling the global SED, consider also the component of radiation from the irradiated accretion disk proposed by Popham & di Stefano (1996). Its possible contribution in the far-UV will reduce the radiation from the burning WD here, and thus its bolometric luminosity, and amount of the required absorption.

These tasks present new challenges for further observations and theoretical modeling, which should help us in understanding the nature and evolutionary status of the most luminous SSSs.

The author thanks the anonymous referee for constructive comments. This research is based on observations made with the Far Ultraviolet Spectroscopic Explorer, International Ultraviolet Explorer obtained from the MAST data archive at the Space Telescope Science Institute, which is operated by the Association of Universities for Research in Astronomy, Inc., under NASA contract NAS 5-26555, and on observations made with the NASA/ESA Hubble Space Telescope, and obtained from the Hubble Legacy Archive, which is a collaboration between the Space Telescope Science Institute (STScI/NASA), the Space Telescope European Coordinating Facility (ST-ECF/ESAC/ESA) and the Canadian Astronomy Data Centre (CADC/NRC/CSA). *DENIS* is the result of a joint effort involving human and financial contributions of several Institutes mostly located in Europe. It has been supported financially mainly by the French Institut National des Sciences de l'Univers, CNRS, and French Education Ministry, the European Southern Observatory, the State of Baden-Wuerttemberg, and the European Commission under networks of the SCIENCE and Human Capital and Mobility programs, the Landessternwarte, Heidelberg and Institut d'Astrophysique de Paris. This publication makes use of data products from the Two Micron All Sky Survey, which is a joint project of the University of Massachusetts and the Infrared Processing and Analysis Center/California Institute of Technology, funded by the National Aeronautics and Space Administration and the National Science Foundation.

This research was supported by the Slovak Research and Development Agency under the contracts No. APVV-15-0458 and APVV-20-0148, and by the Slovak Academy of Sciences grant VEGA No. 2/0030/21.

*Facilities:* ROSAT(PSPC), XMM-Newton, Chandra, FUSE, HST(GHRS, FOS), IUE(SWP, LWP), USNO-B Catalog, NOMAD Catalog, 2MASS All-Sky Catalog, IRSF Magellanic Clouds Point Source Catalog,

2MASS 6X Point Source Working Database/Catalog, The SMC Stellar Catalog and Extinction Map, The LMC Stellar Catalog and Extinction Map, Catalogue of Stellar Spectral Classifications, the 3rd release of the DENIS database

## APPENDIX

### A. JUSTIFICATION OF NEBULAR CONTINUUM IN THE SPECTRUM OF THE SUPERSOFT X-RAY SOURCES

The nebular component of radiation has not yet been considered in modeling the SED of SSSs. We mean the spatially unresolved source of nebular emission, the presence of which in the spectrum is indicated by multiwavelength modeling of the SED (Sect. 3.1 and Fig. 1) as in the case of dense nebulae in symbiotic binaries and/or classical novae (see Skopal 2005, 2015, 2019, Sect. 4.5 here). Its presence also in the spectrum of SSSs can be justified as follows.

1. It is probable that extremely luminous and hot SSSs will generate an outflow of material driven by radiation pressure as it is observed and theoretically justified for luminous hot stars (e.g., Castor et al. 1975; Klein & Castor 1978), accreting WDs in symbiotic binaries (e.g., Vogel & Nussbaumer 1994; Skopal 2006; Skopal et al. 2017), classical novae (e.g., Friedjung 1966; Bath & Shaviv 1976; Kato & Hachisu 1994; Skopal 2019), and in SSSs (e.g., Pakull et al. 1985, 1993; Charles et al. 2010; Oliveira et al. 2010). Simultaneously, the hot and luminous central WD and the boundary layer of accretion disk generate a large flux of hydrogen ionizing photons ( $\sim 10^{48} \text{ s}^{-1}$  for  $T_{\text{BB}} \sim 300\,000 \text{ K}$  and  $L_{\text{SSS}} \sim 10^{38} \text{ erg s}^{-1}$ ), which ionizes the out-flowing material giving rise to nebular emission. This reprocessed radiation dominates the Rayleigh-Jeans tail of a hot source radiating at  $T_{\text{BB}} \gtrsim 10^5 \text{ K}$ , usually from the near-UV to longer wavelengths (see Skopal 2005; Nielsen & Gilfanov 2015). This nebular component of radiation is aimed on explaining the strong UV–NIR excess observed for bright SSSs.
2. Below we summarize indications of the nebular emission observed in the spectrum of our targets.
  - Mass-loss from the accreting nuclear-burning WD is indicated by P-Cyg profiles of H lines, their often strong flux and broad emission wings, and/or satellite components to main  $\text{H}\beta$  and  $\text{He II } \lambda 4686$  emission cores as for RX J0513.9-6951 (see references above and those in Sects. 1.1 to 1.4). Therefore, the  $\text{H}\alpha$  line flux as a tracer of mass loss from hot stars has been usually used to estimate its rate (e.g., Klein & Castor 1978; Leitherer 1988; Lamers & Cassinelli 1999; Skopal et al. 2002; Skopal 2006). The out-flowing material ionized by the central hot source then gives rise to nebular emission.
  - During the optical high state of RX J0513.9-6951, the resonance  $\text{O VI } \lambda 1032, \lambda 1038$  doublet shows broad wings due to electron scattering, with the superposed central P Cyg-type of the profile (see Hutchings et al. 2005). By comparison with accreting nuclear-burning WDs in symbiotic stars, such the wings are created in the layer of electrons, throughout which the line photons are transferred, with the electron optical depth  $\tau_e \sim 0.05 - 0.6$ , depending on the system and its activity (see Sekeráš & Skopal 2012, and Fig. 7 here for illustration). As there is no resolved ionization nebula surrounding RX J0513.9-6951, the layer of free electrons has to be spread in the vicinity of the ionizing source, which indicates the presence of a compact (unresolved) circumstellar nebula in RX J0513.9-6951, independently to our SED model. For a comparison, in the case of the X-ray symbiotic binary AG Dra the layer of scattering electrons extends to  $\approx 10 - 100 R_{\odot}$ , which corresponds to the mean electron concentrations of  $10^{10} - 10^{12} \text{ cm}^{-3}$  to satisfy the measured  $\tau_e$  (see Skopal et al. 2009a).
  - The presence of emission lines directly indicates the presence of the corresponding nebular continuum, because both continuum and lines originate in the same ionized volume. Example here is the case of RX J0058.6-7135 (LIN 333), for which Aller et al. (1987) revealed the presence of a strong nebular emission radiating at a high  $T_e \sim 30000 \text{ K}$ . In particular, the measured (extinction free) flux in the  $\text{H}\beta$  line,  $F_{\text{H}\beta} = 1.45 \times 10^{-13} \text{ erg cm}^{-2} \text{ s}^{-1}$  corresponds to the emission measure,

$$EM = 4\pi d^2 \frac{F_{\text{H}\beta}}{h\nu_{\beta} \alpha(\text{H}\beta)} = 1.4 \times 10^{60} (d/60 \text{ kpc})^2 \text{ cm}^{-3}, \quad (\text{A1})$$

which agrees well with our value determined from the nebular continuum (see Table 3)<sup>3</sup>. In Eq. (A1), we used an effective recombination coefficient for the H $\beta$  transition and  $T_e = 30000$  K,  $\alpha(\text{H}\beta) = 1.088 \times 10^{-14} \text{ cm}^3 \text{ s}^{-1}$  (Hummer & Storey 1987).

- Often measured flux ratio  $F(\text{He II } \lambda 4686)/F(\text{H}\beta) \gg 1$  suggests the presence of the nebular continuum from doubly ionized helium, we can indicate as a discontinuity at  $\sim 2050 \text{ \AA}$  (see Figs. 1c, 2a and 8).
- In spite that the He<sup>++</sup> region around strong SSSs should be especially prominent as compared to other astrophysical nebulae (Rappaport et al. 1994), its presence within the resolved ionization nebula around CAL 83 had not been detected for a long time (Remillard et al. 1995). The first evidence of an He II  $\lambda 4686$  region around CAL 83 was presented by Gruyters et al. (2012) as a faint (relative to its bright stellar component) asymmetrically distributed zone confined to one side of CAL 83. In addition, the authors found that the H II emission did not fit in with model predictions. This unusual He II  $\lambda 4686$  nebular emission could be explained by the presence of a compact (unresolved) circumstellar nebula around the burning WD of CAL 83, whose He<sup>++</sup> zone is almost ionization-bounded, i.e., almost all photons with  $\lambda < 228 \text{ \AA}$  are absorbed within this zone. For a comparison, in the case of the eclipsing symbiotic star AX Per, the He<sup>++</sup> region extends up to  $\sim 50 R_\odot$  from the WD within its dense wind escaping at a rate of  $\sim 2 \times 10^{-6} M_\odot \text{ yr}^{-1}$  and generating the total emission measure of a few times  $10^{59} \text{ cm}^{-3}$  (from the eclipse profile, see Skopal et al. 2011).
- Similarly to the above point, the circumstellar nebulae in the brightest SSSs as suggested by our SED models could attenuate also the flux of H-ionizing photons to such an extent that it would not allow us to detect the corresponding extended ISM nebulae in the optical. From this point of view, the strange absence of ionization ISM nebulae surrounding the brightest SSSs in LMC and SMC, up to CAL 83 (Remillard et al. 1995; Woods & Gilfanov 2016; Farias et al. 2020) could be explained by the presence of compact (unresolved) circumstellar nebulae in these objects.

## B. CAL 83: THE SED OF THE CENTRAL SOURCE AND THE SURROUNDING NEBULA

Figure 8 shows the UV–optical part of the CAL 83 SED compared with that of the surrounding inner  $7.5 \times 7.5 \text{ pc}^2$  ionization nebula. The fluxes of the latter (red crosses in the figure) were taken from Fig. 2 of Gruyters et al. (2012). The spectrum of the outer nebula can be matched with the same type of the nebular continuum (dotted green line) as the circumstellar nebula (solid green line), but scaled with a factor of  $\sim 17$  times larger. This suggests similar electron temperature ( $\sim 30000$  K), but  $\sim 17$  times larger emission measure (i.e.,  $\sim 4.9 \times 10^{61} \text{ cm}^{-3}$ ) in comparison with the dense circumstellar nebula (see Table 3, Sect. 4.5).

As noted above, there is a lack of doubly ionized helium in the surrounding resolved nebula (Appendix A). Therefore, we also compared its fluxes with the net hydrogen nebular continuum that corresponds to  $EM \sim 8.0 \times 10^{61} \text{ cm}^{-3}$  and the same  $T_e$  (gray line in Fig. 8). Such the high  $EM$  requires a high flux of the ionizing photons. Assuming that all H-ionizing photons from CAL 83 balances the rate of recombinations in both nebulae, we can estimate the corresponding  $L_{\text{SSS}}$  for the temperature of the ionizing source  $T_{\text{BB}}$  according to expression,

$$L_{\text{SSS}} = \alpha_{\text{B}}(\text{H}, T_e) EM \frac{\sigma T_{\text{BB}}^4}{f(T_{\text{BB}})}, \quad (\text{B2})$$

(see Skopal et al. 2017), where the function  $f(T_{\text{BB}})$  determines the flux of ionizing photons emitted by  $1 \text{ cm}^2$  area of the ionizing source, and  $\alpha_{\text{B}}(\text{H}, T_e)$  is the recombination coefficient to all but the ground state of hydrogen (i.e., Case B). Then the total  $EM \sim 8.29 \times 10^{61} \text{ cm}^{-3}$  (i.e., of both nebulae),  $T_{\text{BB}} = 345000 \text{ K}$ ,  $f(T_{\text{BB}}) = 6.0 \times 10^{27} \text{ cm}^{-2} \text{ s}^{-1}$ , and  $\alpha_{\text{B}}(\text{H}, 30000) = 9.97 \times 10^{-14} \text{ cm}^3$  (Nussbaumer & Vogel 1987) correspond to  $L_{\text{SSS}} \sim 1.1 \times 10^{39} \text{ erg s}^{-1}$ . This value is close to that given by the SED models, but in the order of magnitude higher than those derived from the emission lines in previous works (see Sect. 1.3). Consequently, the very high  $EM$  ( $8.0 \times 10^{61} \text{ cm}^{-3}$ ) of the  $7.5 \times 7.5 \text{ pc}^2$  nebula surrounding CAL 83 corresponds to its average particle density  $\sim 39 \text{ cm}^{-3}$  and the mass of  $\sim 1700 M_\odot$ , which are a factor of  $>4$ , and a factor of  $\sim 11$ , respectively, larger than those previously derived from emission lines (e.g.,

<sup>3</sup> Note that values of parameters derived from the emission lines are usually smaller than those derived from the continuum, because nebulae are usually more opaque in the lines than in the continuum.

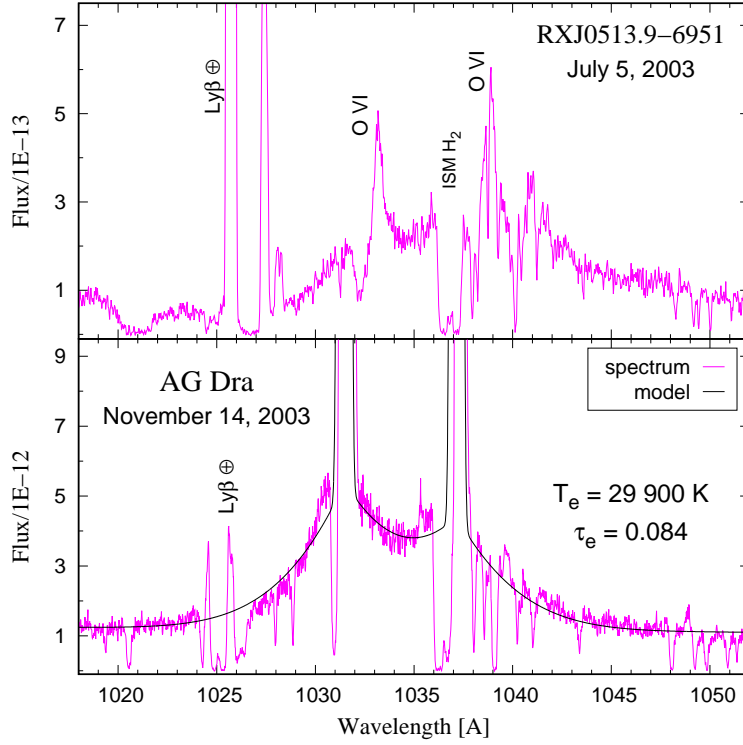


**Figure 7.** Broad wings of the resonance O VI  $\lambda 1032$ ,  $\lambda 1038$  doublet observed in the *FUSE* spectra of LMC SSS RX J0513.9-6951 (top panel) and of the X-ray symbiotic binary AG Dra with the model of the scattering of line photons on free electrons (bottom panel, adopted from Sekeráš & Skopal 2012). The similarity of these profiles suggests the presence of a dense circumstellar nebula also in RX J0513.9-6951, showing mass-outflow (see text). Note that the spectra of RX J0513.9-6951 and AG Dra are shifted in wavelengths due to their space velocity by  $\sim +500$  and  $\sim -150$   $\text{km s}^{-1}$ , respectively (Hutchings et al. 2005; Fekel et al. 2000).

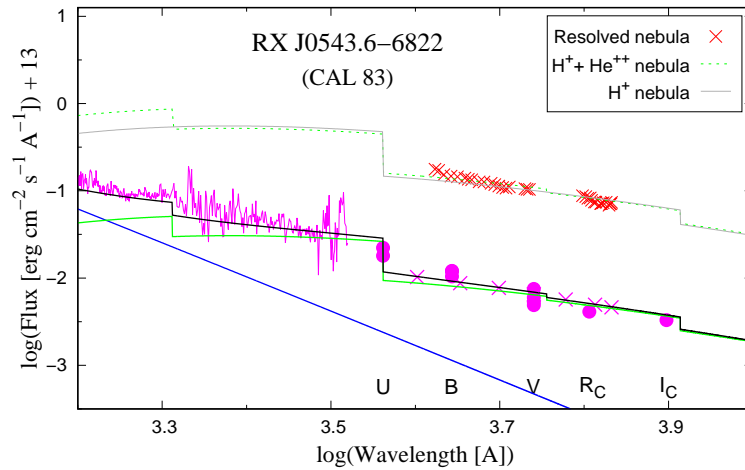


**Figure 8.** The UV–optical part of the CAL 83 SED from Fig. 1c including representative flux-points from the resolved  $7.5 \times 7.5$   $\text{pc}^2$  nebula surrounding CAL 83 (red crosses), taken from Fig. 2 of Gruyters et al. (2012). They can be matched by nebular continuum with the same  $T_e$  but significantly larger  $EM$  (dotted green and gray line for  $\text{H}^+ + \text{He}^{++}$  and  $\text{H}^+$  nebula) than the unresolved circumstellar nebula (solid green line; see text). Meaning of the other lines and symbols as in Fig. 1.

Remillard et al. 1995; Gruyters et al. 2012). Such the large difference of the surrounding nebula properties can be given by a large difference in the opacity of the emitting medium in the line and the continuum transitions, respectively.

**Table 4.** Luminosities of the strongest permitted lines in the UV spectrum (in  $\text{erg s}^{-1}$ ), emission measure  $EM$  ( $\text{cm}^{-3}$ ), and electron temperature  $T_e$  (K) of LIN 333 and SY Mus. The distance dependent parameters are scaled with 1.0 kpc (Skopal 2005) and 60 kpc for SY Mus and LIN 333, respectively. The corresponding spectra and models are shown in Fig. 9a and 9b.

Object	$L_{\text{NV } \lambda 1240}$	$L_{\text{C IV } \lambda 1550}$	$L_{\text{He II } \lambda 1640}$	$EM$	$T_e$
LIN 333	$2.7 \times 10^{35}$	$5.4 \times 10^{34}$	$2.9 \times 10^{35}$	$1.6 \times 10^{60}$	$\sim 37000$
SY Mus	$2.1 \times 10^{34}$	$2.2 \times 10^{34}$	$1.1 \times 10^{34}$	$3 \times 10^{59}$	$\sim 18500$

### C. LIN 333: PLANETARY NEBULA OR A BINARY SYSTEM?

Here we present two reasons suggesting that LIN 333 could be a binary system.

(i) First, we compare the nebular spectrum, both in the continuum and emission lines, of LIN 333 with that observed in symbiotic binaries containing an accreting nuclear-burning WD. Panels **a** and **b** of Fig. 9 show a comparison with SY Mus in the 1200 – 2200 Å part of the spectrum. Both, LIN 333 and SY Mus contain the same emission lines in the far-UV spectrum, except for the low-excitation O I  $\lambda\lambda 1302$ -1306 lines<sup>4</sup>, which are characteristic for symbiotic stars. Strong resonance emission lines, NV  $\lambda\lambda 1238, 1242$ , C IV  $\lambda\lambda 1548, 1550$ , high-ionization line He II  $\lambda 1640$ , and the intersystem lines of O IV]  $\lambda\lambda 1397$ -1405, N IV]  $\lambda\lambda 1483$ -1486, O III]  $\lambda\lambda 1661, 1666$ , N III]  $\lambda\lambda 1746$ -1753, Si III  $\lambda 1892$  and C III  $\lambda\lambda 1907, 1909$  reflect the circumstellar nebular conditions of symbiotic stars (Meier et al. 1994), and thus also of SSS LIN 333.

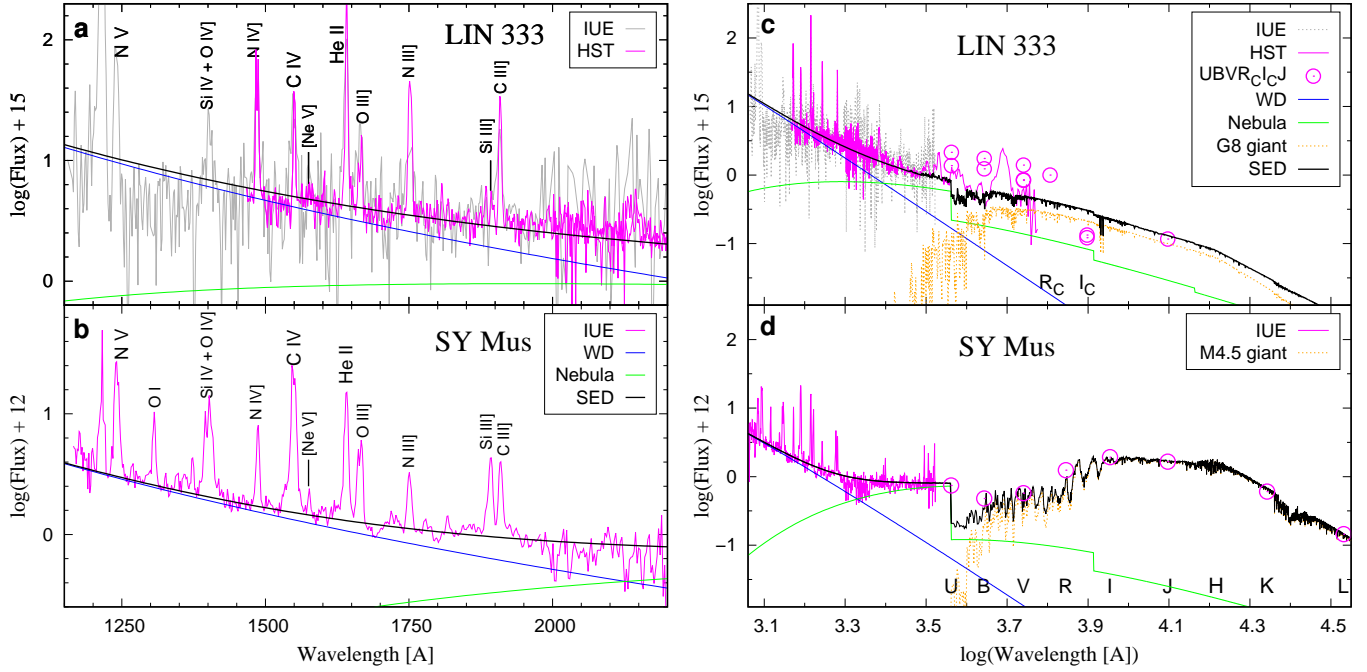
Also, the nebular continuum in the LIN 333 spectrum is unambiguously indicated by our method as for other targets (green lines in Fig. 1). As there is no resolved ionization nebula around LIN 333, the indicated nebular continuum suggests the presence of a compact unresolved nebula in the system, the origin of which is similar to that of dense symbiotic nebulae, i.e., resulting from the interaction between the binary components, given by the ionized mass outflows (e.g., Boyarchuk et al. 1966; Seaquist et al. 1984; Nussbaumer & Vogel 1987; Skopal 2005). Here, it is of interest to note that the first studies of symbiotic stars pointed to the similarity of their hot components to the central star of planetary nebulae (e.g., Berman 1932), and this possibility was often considered until the first satellite observations that unambiguously revealed the binary nature of symbiotic stars (e.g., Kenyon & Webbink 1984, and references therein).

Table 4 compares luminosities of the strongest emission lines in the UV spectrum,  $EM$  and  $T_e$  of the compact nebulae of LIN 333 and SY Mus.

(ii) According to the  $UBV$  photometry and the  $HST$  spectroscopy of LIN 333 (Sect. 2.2), the measured fluxes in the visual band lie above our two-components model (see Fig. 1b), which suggests contribution from the companion in a binary system. To match the optical continuum of the  $HST$  spectrum<sup>5</sup> with a minimum effect on the near-UV region, where the original two-component model is satisfactory (see Fig. 1b), we selected a synthetic spectrum of a yellow giant from a grid of models made by Hauschildt et al. (1999), calculated for  $T_{\text{eff}} = 5000 \text{ K}$ ,  $\log g = 3.5$  and  $[M/H] = -1$ . Its scaling in Fig. 9c corresponds to the luminosity of  $278 L_{\odot}$  and the radius of  $22 R_{\odot}$ ; parameters similar to a G8 III giant (e.g., van Belle et al. 1999). If this were the case, LIN 333 would belong to the so-called yellow symbiotic stars. However, new optical/NIR observations are highly desirable to confirm or refute the binary nature of LIN 333.

<sup>4</sup> The absence of O I and very faint resonance O VI  $\lambda\lambda 1032, 1038$  doublet probably reflect a low abundance of oxygen in the LIN 333 nebula suggested by Leisy & Dennefeld (1996).

<sup>5</sup> We ignored the  $U, B, V$  fluxes, because they are not corrected for emission lines, and thus lie well above the true continuum.



**Figure 9.** Left: Comparison of the far-UV spectrum emitted by the SSS LIN 333 (a) and by the symbiotic binary SY Mus (b), dereddened with  $E_{B-V} = 0.08$  and  $0.35$ . The similarity of the nebular spectrum of both systems suggests their same origin – in a compact circumstellar nebula (see text). Right: The UV–NIR SEDs of these objects. The case of LIN 333 allows the presence of a yellow giant companion (orange dashed line) to the SSS, suggesting binary nature of LIN 333 (see Appendix C). Panels a and c represent details of Fig. 1b, while the panels b and d were adapted according to Fig. 18 of Skopal (2005).

## REFERENCES

- Alcock, C., Allsman, R. A., Alves, D., et al. 1996, *Mon. Not. R. Astron. Soc.*, 280, L49, doi: [10.1093/mnras/280.3.L49](https://doi.org/10.1093/mnras/280.3.L49)
- Alcock, C., Allsman, R. A., Alves, D. R., et al. 1997, *Mon. Not. R. Astron. Soc.*, 291, L13, doi: [10.1093/mnras/291.1.L13](https://doi.org/10.1093/mnras/291.1.L13)
- Aller, L. H., Keyes, C. D., Maran, S. P., et al. 1987, *Astrophys. J.*, 320, 159, doi: [10.1086/165532](https://doi.org/10.1086/165532)
- Aydi, E., Page, K. L., Kuin, N. P. M., et al. 2018, *Mon. Not. R. Astron. Soc.*, 474, 2679, doi: [10.1093/mnras/stx2678](https://doi.org/10.1093/mnras/stx2678)
- Bath, G. T., & Shaviv, G. 1976, *MNRAS*, 175, 305, doi: [10.1093/mnras/175.2.305](https://doi.org/10.1093/mnras/175.2.305)
- Becker, C. M., Remillard, R. A., Rappaport, S. A., & McClintock, J. E. 1998, *Astrophys. J.*, 506, 880, doi: [10.1086/306272](https://doi.org/10.1086/306272)
- Berman, L. 1932, *PASP*, 44, 318, doi: [10.1086/124255](https://doi.org/10.1086/124255)
- Bernard-Salas, J., Peeters, E., Sloan, G. C., et al. 2009, *ApJ*, 699, 1541, doi: [10.1088/0004-637X/699/2/1541](https://doi.org/10.1088/0004-637X/699/2/1541)
- Bessell, M. S. 1979, *Publ. Astron. Soc. Pac.*, 91, 589, doi: [10.1086/130542](https://doi.org/10.1086/130542)
- Bohm, D., & Aller, L. H. 1947, *ApJ*, 105, 131, doi: [10.1086/144890](https://doi.org/10.1086/144890)
- Boyarchuk, A. A., Esipov, V. F., & Moroz, V. I. 1966, *Soviet Ast.*, 10, 331
- Burwitz, V., Reinsch, K., Greiner, J., et al. 2008, *Astron. Astrophys.*, 481, 193, doi: [10.1051/0004-6361:20067010](https://doi.org/10.1051/0004-6361:20067010)
- Carpano, S., Haberl, F., & Maitra, C. 2019, *Mon. Not. R. Astron. Soc.*, 490, 4804, doi: [10.1093/mnras/stz2940](https://doi.org/10.1093/mnras/stz2940)
- Castor, J. I., Abbott, D. C., & Klein, R. I. 1975, *ApJ*, 195, 157, doi: [10.1086/153315](https://doi.org/10.1086/153315)
- Charles, P. A., McGowan, K. E., Blustin, A. J., et al. 2010, *NewAR*, 54, 75, doi: [10.1016/j.newar.2010.09.003](https://doi.org/10.1016/j.newar.2010.09.003)
- Cowley, A. P., Crampton, D., Hutchings, J. B., et al. 1984, *Astrophys. J.*, 286, 196, doi: [10.1086/162587](https://doi.org/10.1086/162587)
- Cowley, A. P., Schmidtke, P. C., Crampton, D., & Hutchings, J. B. 2002, *Astron. J.*, 124, 2233, doi: [10.1086/342852](https://doi.org/10.1086/342852)
- Cowley, A. P., Schmidtke, P. C., McGrath, T. K., et al. 1997, *Publ. Astron. Soc. Pac.*, 109, 21, doi: [10.1086/133855](https://doi.org/10.1086/133855)
- Crampton, D., Cowley, A. P., Hutchings, J. B., et al. 1987, *Astrophys. J.*, 321, 745, doi: [10.1086/165667](https://doi.org/10.1086/165667)
- Crampton, D., Hutchings, J. B., Cowley, A. P., et al. 1996, *Astrophys. J.*, 456, 320, doi: [10.1086/176653](https://doi.org/10.1086/176653)
- Crudace, R., Paresce, F., Bowyer, S., & Lampton, M. 1974, *Astrophys. J.*, 187, 497, doi: [10.1086/152659](https://doi.org/10.1086/152659)
- Farias, D. A., Clocchiatti, A., Woods, T. E., & Rest, A. 2020, *MNRAS*, 497, 3234, doi: [10.1093/mnras/staa2213](https://doi.org/10.1093/mnras/staa2213)
- Fekel, F. C., Hinkle, K. H., Joyce, R. R., & Skrutskie, M. F. 2000, *AJ*, 120, 3255, doi: [10.1086/316872](https://doi.org/10.1086/316872)
- Fender, R. P., Stirling, A. M., Spencer, R. E., et al. 2006, *Mon. Not. R. Astron. Soc.*, 369, 603, doi: [10.1111/j.1365-2966.2006.10193.x](https://doi.org/10.1111/j.1365-2966.2006.10193.x)
- Freeland, M., Kuncic, Z., Soria, R., & Bicknell, G. V. 2006, *Mon. Not. R. Astron. Soc.*, 372, 630, doi: [10.1111/j.1365-2966.2006.10750.x](https://doi.org/10.1111/j.1365-2966.2006.10750.x)
- Friedjung, M. 1966, *MNRAS*, 132, 317, doi: [10.1093/mnras/132.2.317](https://doi.org/10.1093/mnras/132.2.317)
- . 1987, *Astron. Astrophys.*, 179, 164
- Fujimoto, M. Y. 1982, *Astrophys. J.*, 257, 767, doi: [10.1086/160030](https://doi.org/10.1086/160030)
- Gänsicke, B. T., Beuermann, K., & de Martino, D. 1996, *Phase Resolved UV Spectroscopy of RX J0019.8+2156*, ed. J. Greiner, Vol. 472, 107, doi: [10.1007/BFb0102252](https://doi.org/10.1007/BFb0102252)
- Gänsicke, B. T., van Teeseling, A., Beuermann, K., & de Martino, D. 1998, *Astron. Astrophys.*, 333, 163
- Gladstone, J. C., Roberts, T. P., & Done, C. 2009, *Mon. Not. R. Astron. Soc.*, 397, 1836, doi: [10.1111/j.1365-2966.2009.15123.x](https://doi.org/10.1111/j.1365-2966.2009.15123.x)
- González-Riestra, R., Viotti, R. F., Iijima, T., et al. 2008, *A&A*, 481, 725, doi: [10.1051/0004-6361:20078593](https://doi.org/10.1051/0004-6361:20078593)
- Greiner, J., & Di Stefano, R. 2002, *Astron. Astrophys.*, 387, 944, doi: [10.1051/0004-6361:20020463](https://doi.org/10.1051/0004-6361:20020463)
- Greiner, J., Hasinger, G., & Kahabka, P. 1991, *Astron. Astrophys.*, 246, L17
- Greiner, J., Schwarz, R., Hasinger, G., & Orio, M. 1996, *Astron. Astrophys.*, 312, 88
- Gruyters, P., Exter, K., Roberts, T. P., & Rappaport, S. 2012, *A&A*, 544, A86, doi: [10.1051/0004-6361/201219051](https://doi.org/10.1051/0004-6361/201219051)
- Gurzadyan, G. A. 1997, *The Physics and Dynamics of Planetary Nebulae*
- Hachisu, I., & Kato, M. 2001, *Astrophys. J.*, 558, 323, doi: [10.1086/321601](https://doi.org/10.1086/321601)
- Hauschildt, P. H., Allard, F., Ferguson, J., Baron, E., & Alexander, D. R. 1999, *ApJ*, 525, 871, doi: [10.1086/307954](https://doi.org/10.1086/307954)
- Heise, J., van Teeseling, A., & Kahabka, P. 1994, *Astron. Astrophys.*, 288, L45
- Henden, A. A., & Kaitchuck, R. H. 1982, *Astronomical photometry*
- Henize, K. G. 1956, *Astrophys. J. Suppl. Ser.*, 2, 315, doi: [10.1086/190025](https://doi.org/10.1086/190025)
- Henze, M., Darnley, M. J., Williams, S. C., et al. 2018, *Astrophys. J.*, 857, 68, doi: [10.3847/1538-4357/aab6a6](https://doi.org/10.3847/1538-4357/aab6a6)
- Hummer, D. G., & Storey, P. J. 1987, *MNRAS*, 224, 801, doi: [10.1093/mnras/224.3.801](https://doi.org/10.1093/mnras/224.3.801)

- Hutchings, J. B., Cowley, A. P., Mann, R., Schmidtke, P. C., & Crampton, D. 2005, *AJ*, 129, 2792, doi: [10.1086/430147](https://doi.org/10.1086/430147)
- Hutchings, J. B., Winter, K., Cowley, A. P., Schmidtke, P. C., & Crampton, D. 2002, *Astron. J.*, 124, 2833, doi: [10.1086/343839](https://doi.org/10.1086/343839)
- Irwin, J. A., Bregman, J. N., & Athey, A. E. 2004, *Astrophys. J. Letters*, 601, L143, doi: [10.1086/382026](https://doi.org/10.1086/382026)
- Jin, J., Feng, H., & Kaaret, P. 2010, *Astrophys. J.*, 716, 181, doi: [10.1088/0004-637X/716/1/181](https://doi.org/10.1088/0004-637X/716/1/181)
- Kahabka, P. 1998, *Astron. Astrophys.*, 331, 328
- Kahabka, P., Pietsch, W., & Hasinger, G. 1994, *A&A*, 288, 538
- Kahabka, P., & van den Heuvel, E. P. J. 1997, *Annual Rev. Astron. Astrophys.*, 35, 69, doi: [10.1146/annurev.astro.35.1.69](https://doi.org/10.1146/annurev.astro.35.1.69)
- Kato, D., Nagashima, C., Nagayama, T., et al. 2007, *Publ. Astron. Soc. Japan*, 59, 615, doi: [10.1093/pasj/59.3.615](https://doi.org/10.1093/pasj/59.3.615)
- Kato, M., & Hachisu, I. 1994, *Astrophys. J.*, 437, 802, doi: [10.1086/175041](https://doi.org/10.1086/175041)
- Kato, M., Saio, H., & Hachisu, I. 2017, *Astrophys. J.*, 838, 153, doi: [10.3847/1538-4357/838/2/153](https://doi.org/10.3847/1538-4357/838/2/153)
- Kenyon, S. J., & Webbink, R. F. 1984, *ApJ*, 279, 252, doi: [10.1086/161888](https://doi.org/10.1086/161888)
- King, A. R. 2008, *Mon. Not. R. Astron. Soc.*, 385, L113, doi: [10.1111/j.1745-3933.2008.00444.x](https://doi.org/10.1111/j.1745-3933.2008.00444.x)
- Klein, R. I., & Castor, J. I. 1978, *ApJ*, 220, 902, doi: [10.1086/155980](https://doi.org/10.1086/155980)
- Kong, A. K. H., & Di Stefano, R. 2003, *Astrophys. J. Letters*, 590, L13, doi: [10.1086/376552](https://doi.org/10.1086/376552)
- Kovetz, A., Prialnik, D., & Shara, M. M. 1988, *Astrophys. J.*, 325, 828, doi: [10.1086/166053](https://doi.org/10.1086/166053)
- Kuuttila, J., Gilfanov, M., Woods, T. E., Seitenzahl, I. R., & Ruiter, A. J. 2021, *Mon. Not. R. Astron. Soc.*, 500, 3763, doi: [10.1093/mnras/staa3485](https://doi.org/10.1093/mnras/staa3485)
- Lamers, H. J. G. L. M., & Cassinelli, J. P. 1999, *Introduction to Stellar Winds*
- Lanz, T., Telis, G. A., Audard, M., et al. 2005, *Astrophys. J.*, 619, 517, doi: [10.1086/426382](https://doi.org/10.1086/426382)
- Leisy, P., & Dennefeld, M. 1996, *A&AS*, 116, 95
- Leitherer, C. 1988, *ApJ*, 326, 356, doi: [10.1086/166097](https://doi.org/10.1086/166097)
- Lewis, H. M., Anguiano, B., Stassun, K. G., et al. 2020, *Astrophys. J. Letters*, 900, L43, doi: [10.3847/2041-8213/abb248](https://doi.org/10.3847/2041-8213/abb248)
- Lindsay, E. M. 1961, *Astron. J.*, 66, 169, doi: [10.1086/108396](https://doi.org/10.1086/108396)
- Liu, J.-F., Bai, Y., Wang, S., et al. 2015, *Nature*, 528, 108, doi: [10.1038/nature15751](https://doi.org/10.1038/nature15751)
- Livio, M. 1997, in *Astronomical Society of the Pacific Conference Series*, Vol. 121, IAU Colloq. 163: *Accretion Phenomena and Related Outflows*, ed. D. T. Wickramasinghe, G. V. Bicknell, & L. Ferrario, 845
- Long, K. S., Helfand, D. J., & Grabelsky, D. A. 1981, *Astrophys. J.*, 248, 925, doi: [10.1086/159222](https://doi.org/10.1086/159222)
- Masetti, N., Rigon, E., Maiorano, E., et al. 2007a, *Astron. Astrophys.*, 464, 277, doi: [10.1051/0004-6361:20066517](https://doi.org/10.1051/0004-6361:20066517)
- Masetti, N., Landi, R., Pretorius, M. L., et al. 2007b, *Astron. Astrophys.*, 470, 331, doi: [10.1051/0004-6361:20077509](https://doi.org/10.1051/0004-6361:20077509)
- Massey, P. 2002, *Astrophys. J. Suppl. Ser.*, 141, 81, doi: [10.1086/338286](https://doi.org/10.1086/338286)
- Mateo, M. L. 1998, *Annual Rev. Astron. Astrophys.*, 36, 435, doi: [10.1146/annurev.astro.36.1.435](https://doi.org/10.1146/annurev.astro.36.1.435)
- Meier, S. R., Kafatos, M., Fahey, R. P., & Michalitsianos, A. G. 1994, *ApJS*, 94, 183, doi: [10.1086/192078](https://doi.org/10.1086/192078)
- Mereghetti, S., Krachmalnicoff, N., La Palombara, N., et al. 2010, *Astron. Astrophys.*, 519, A42, doi: [10.1051/0004-6361/201014430](https://doi.org/10.1051/0004-6361/201014430)
- Mirabel, I. F., & Rodríguez, L. F. 1999, *Annual Rev. Astron. Astrophys.*, 37, 409, doi: [10.1146/annurev.astro.37.1.409](https://doi.org/10.1146/annurev.astro.37.1.409)
- Monet, D. G., Levine, S. E., Canzian, B., et al. 2003, *Astron. J.*, 125, 984, doi: [10.1086/345888](https://doi.org/10.1086/345888)
- Motch, C., Pakull, M. W., Soria, R., Grisé, F., & Pietrzyński, G. 2014, *Nature*, 514, 198, doi: [10.1038/nature13730](https://doi.org/10.1038/nature13730)
- Muerset, U., Nussbaumer, H., Schmid, H. M., & Vogel, M. 1991, *A&A*, 248, 458
- Mukai, K. 2017, *Publ. Astron. Soc. Pac.*, 129, 062001, doi: [10.1088/1538-3873/aa6736](https://doi.org/10.1088/1538-3873/aa6736)
- Ness, J. U., Schwarz, G., Starrfield, S., et al. 2008, *Astron. J.*, 135, 1328, doi: [10.1088/0004-6256/135/4/1328](https://doi.org/10.1088/0004-6256/135/4/1328)
- Nielsen, M. T. B., & Gilfanov, M. 2015, *MNRAS*, 453, 2927, doi: [10.1093/mnras/stv1616](https://doi.org/10.1093/mnras/stv1616)
- Nussbaumer, H., Schmid, H. M., & Vogel, M. 1989, *Astron. Astrophys.*, 211, L27
- Nussbaumer, H., & Vogel, M. 1987, *A&A*, 182, 51
- Odendaal, A., & Meintjes, P. J. 2017, *Mon. Not. R. Astron. Soc.*, 467, 2797, doi: [10.1093/mnras/stx233](https://doi.org/10.1093/mnras/stx233)
- Odendaal, A., Meintjes, P. J., Charles, P. A., & Rajoelimanana, A. F. 2014, *Mon. Not. R. Astron. Soc.*, 437, 2948, doi: [10.1093/mnras/stt2111](https://doi.org/10.1093/mnras/stt2111)
- Oegelman, H., Orio, M., Krautter, J., & Starrfield, S. 1993, *Nature*, 361, 331, doi: [10.1038/361331a0](https://doi.org/10.1038/361331a0)
- Oliveira, A. S., Steiner, J. E., Ricci, T. V., Menezes, R. B., & Borges, B. W. 2010, *Astron. Astrophys.*, 517, L5, doi: [10.1051/0004-6361/201014773](https://doi.org/10.1051/0004-6361/201014773)

- Orio, M., Hartmann, W., Still, M., & Greiner, J. 2003, *Astrophys. J.*, 594, 435, doi: [10.1086/376828](https://doi.org/10.1086/376828)
- Paczynski, B., & Zytkow, A. N. 1978, *Astrophys. J.*, 222, 604, doi: [10.1086/156176](https://doi.org/10.1086/156176)
- Paerels, F., Rasmussen, A. P., Hartmann, H. W., et al. 2001, *Astron. Astrophys.*, 365, L308, doi: [10.1051/0004-6361:20000069](https://doi.org/10.1051/0004-6361:20000069)
- Pakull, M. W., Ilovaisky, S. A., & Chevalier, C. 1985, *Space Sci. Rev.*, 40, 229, doi: [10.1007/BF00212890](https://doi.org/10.1007/BF00212890)
- Pakull, M. W., & Motch, C. 1989, in *European Southern Observatory Conference and Workshop Proceedings*, Vol. 32, European Southern Observatory Conference and Workshop Proceedings, 285
- Pakull, M. W., Motch, C., Bianchi, L., et al. 1993, *Astron. Astrophys.*, 278, L39
- Panei, J. A., Althaus, L. G., & Benvenuto, O. G. 2000, *Astron. Astrophys.*, 353, 970, <https://arxiv.org/abs/astro-ph/9909499>
- Parmar, A. N., Kahabka, P., Hartmann, H. W., Heise, J., & Taylor, B. G. 1998, *Astron. Astrophys.*, 332, 199, <https://arxiv.org/abs/astro-ph/9712040>
- Popham, R., & di Stefano, R. 1996, *Accretion Disks in Supersoft X-Ray Sources*, ed. J. Greiner, Vol. 472, 65, doi: [10.1007/BFb0102247](https://doi.org/10.1007/BFb0102247)
- Rajoelimanana, A. F., Charles, P. A., Meintjes, P. J., Odendaal, A., & Udalski, A. 2013, *Mon. Not. R. Astron. Soc.*, 432, 2886, doi: [10.1093/mnras/stt645](https://doi.org/10.1093/mnras/stt645)
- Rappaport, S., Chiang, E., Kallman, T., & Malina, R. 1994, *ApJ*, 431, 237, doi: [10.1086/174481](https://doi.org/10.1086/174481)
- Reinsch, K., van Teeseling, A., Beuermann, K., & Abbott, T. M. C. 1996, *Astron. Astrophys.*, 309, L11
- Reinsch, K., van Teeseling, A., King, A. R., & Beuermann, K. 2000, *Astron. Astrophys.*, 354, L37, <https://arxiv.org/abs/astro-ph/0001081>
- Remillard, R. A., Rappaport, S., & Macri, L. M. 1995, *ApJ*, 439, 646, doi: [10.1086/175204](https://doi.org/10.1086/175204)
- Saeedi, S., Sasaki, M., & Ducci, L. 2018, *Mon. Not. R. Astron. Soc.*, 473, 440, doi: [10.1093/mnras/stx2354](https://doi.org/10.1093/mnras/stx2354)
- Sanduleak, N., MacConnell, D. J., & Philip, A. G. D. 1978, *Publ. Astron. Soc. Pac.*, 90, 621, doi: [10.1086/130397](https://doi.org/10.1086/130397)
- Schaeidt, S., Hasinger, G., & Truemper, J. 1993, *Astron. Astrophys.*, 270, L9
- Schmidtke, P. C., Cowley, A. P., Hutchings, J. B., Winter, K., & Crampton, D. 2004, *Astron. J.*, 127, 469, doi: [10.1086/380222](https://doi.org/10.1086/380222)
- Schwarz, G. J., Hauschildt, P. H., Starrfield, S., et al. 1998, *Mon. Not. R. Astron. Soc.*, 300, 931, doi: [10.1046/j.1365-8711.1998.01964.x](https://doi.org/10.1046/j.1365-8711.1998.01964.x)
- Schwarz, G. J., Shore, S. N., Starrfield, S., et al. 2001, *Mon. Not. R. Astron. Soc.*, 320, 103, doi: [10.1046/j.1365-8711.2001.03960.x](https://doi.org/10.1046/j.1365-8711.2001.03960.x)
- Seaquist, E. R., Taylor, A. R., & Button, S. 1984, *ApJ*, 284, 202, doi: [10.1086/162399](https://doi.org/10.1086/162399)
- Sekeráš, M., & Skopal, A. 2012, *MNRAS*, 427, 979, doi: [10.1111/j.1365-2966.2012.21991.x](https://doi.org/10.1111/j.1365-2966.2012.21991.x)
- Seward, F. D., & Mitchell, M. 1981, *Astrophys. J.*, 243, 736, doi: [10.1086/158641](https://doi.org/10.1086/158641)
- Shagatova, N., Skopal, A., & Cariková, Z. 2016, *Astron. Astrophys.*, 588, A83, doi: [10.1051/0004-6361/201525645](https://doi.org/10.1051/0004-6361/201525645)
- Shagatova, N., Skopal, A., Shugarov, S. Y., et al. 2021, *Astron. Astrophys.*, 646, A116, doi: [10.1051/0004-6361/202039103](https://doi.org/10.1051/0004-6361/202039103)
- Shanley, L., Ogelman, H., Gallagher, J. S., Orio, M., & Krautter, J. 1995, *Astrophys. J. Letters*, 438, L95, doi: [10.1086/187724](https://doi.org/10.1086/187724)
- Shen, K. J., & Bildsten, L. 2007, *Astrophys. J.*, 660, 1444, doi: [10.1086/513457](https://doi.org/10.1086/513457)
- Skiff, B. A. 2010, *VizieR Online Data Catalog*, B/mk
- Skopal, A. 2005, *A&A*, 440, 995, doi: [10.1051/0004-6361:20034262](https://doi.org/10.1051/0004-6361:20034262)
- . 2006, *A&A*, 457, 1003, doi: [10.1051/0004-6361:20064935](https://doi.org/10.1051/0004-6361:20064935)
- . 2015, *New Astron.*, 36, 116, doi: [10.1016/j.newast.2013.10.009](https://doi.org/10.1016/j.newast.2013.10.009)
- . 2019, *Astrophys. J.*, 878, 28, doi: [10.3847/1538-4357/ab1f07](https://doi.org/10.3847/1538-4357/ab1f07)
- Skopal, A., Bode, M. F., Crocker, M. M., et al. 2002, *MNRAS*, 335, 1109, doi: [10.1046/j.1365-8711.2002.05715.x](https://doi.org/10.1046/j.1365-8711.2002.05715.x)
- Skopal, A., & Cariková, Z. 2015, *Astron. Astrophys.*, 573, A8, doi: [10.1051/0004-6361/201424779](https://doi.org/10.1051/0004-6361/201424779)
- Skopal, A., Sekeráš, M., González-Riestra, R., & Viotti, R. F. 2009a, *Astron. Astrophys.*, 507, 1531, doi: [10.1051/0004-6361/200811418](https://doi.org/10.1051/0004-6361/200811418)
- Skopal, A., Tarasova, T. N., Wolf, M., Dubovský, P. A., & Kudzej, I. 2018, *Astrophys. J.*, 858, 120, doi: [10.3847/1538-4357/aabc11](https://doi.org/10.3847/1538-4357/aabc11)
- Skopal, A., Teodorani, M., Errico, L., et al. 2001, *A&A*, 367, 199, doi: [10.1051/0004-6361:20000413](https://doi.org/10.1051/0004-6361:20000413)
- Skopal, A., Pribulla, T., Budaj, J., et al. 2009b, *Astrophys. J.*, 690, 1222, doi: [10.1088/0004-637X/690/2/1222](https://doi.org/10.1088/0004-637X/690/2/1222)
- Skopal, A., Tarasova, T. N., Cariková, Z., et al. 2011, *A&A*, 536, A27, doi: [10.1051/0004-6361/201116969](https://doi.org/10.1051/0004-6361/201116969)
- Skopal, A., Drechsel, H., Tarasova, T., et al. 2014, *A&A*, 569, A112, doi: [10.1051/0004-6361/201424284](https://doi.org/10.1051/0004-6361/201424284)
- Skopal, A., Shugarov, S. Y., Sekeráš, M., et al. 2017, *A&A*, 604, A48, doi: [10.1051/0004-6361/201629593](https://doi.org/10.1051/0004-6361/201629593)
- Skrutskie, M. F., Cutri, R. M., Stiening, R., et al. 2006, *Astron. J.*, 131, 1163, doi: [10.1086/498708](https://doi.org/10.1086/498708)

- Smale, A. P., Corbet, R. H. D., Charles, P. A., et al. 1988, *Mon. Not. R. Astron. Soc.*, 233, 51, doi: [10.1093/mnras/233.1.51](https://doi.org/10.1093/mnras/233.1.51)
- Soraisam, M. D., Gilfanov, M., Wolf, W. M., & Bildsten, L. 2016, *Mon. Not. R. Astron. Soc.*, 455, 668, doi: [10.1093/mnras/stv2359](https://doi.org/10.1093/mnras/stv2359)
- Soria, R., & Kong, A. 2016, *Mon. Not. R. Astron. Soc.*, 456, 1837, doi: [10.1093/mnras/stv2671](https://doi.org/10.1093/mnras/stv2671)
- Southwell, K. A., Livio, M., Charles, P. A., O'Donoghue, D., & Sutherland, W. J. 1996, *Astrophys. J.*, 470, 1065, doi: [10.1086/177931](https://doi.org/10.1086/177931)
- Takeuchi, S., Ohsuga, K., & Mineshige, S. 2010, *Publ. Astron. Soc. Japan*, 62, L43, doi: [10.1093/pasj/62.5.L43](https://doi.org/10.1093/pasj/62.5.L43)
- Urquhart, R., & Soria, R. 2016, *Mon. Not. R. Astron. Soc.*, 456, 1859, doi: [10.1093/mnras/stv2293](https://doi.org/10.1093/mnras/stv2293)
- van Belle, G. T., Lane, B. F., Thompson, R. R., et al. 1999, *AJ*, 117, 521, doi: [10.1086/300677](https://doi.org/10.1086/300677)
- van den Heuvel, E. P. J., Bhattacharya, D., Nomoto, K., & Rappaport, S. A. 1992, *Astron. Astrophys.*, 262, 97
- Vasilopoulos, G., Koliopanos, F., Woods, T. E., et al. 2020, *Mon. Not. R. Astron. Soc.*, 499, 2007, doi: [10.1093/mnras/staa2922](https://doi.org/10.1093/mnras/staa2922)
- Villaver, E., Stanghellini, L., & Shaw, R. A. 2004, *ApJ*, 614, 716, doi: [10.1086/423832](https://doi.org/10.1086/423832)
- Vogel, M., & Nussbaumer, H. 1994, *A&A*, 284, 145
- Wang, Q. 1991, *Mon. Not. R. Astron. Soc.*, 252, 47P, doi: [10.1093/mnras/252.1.47P](https://doi.org/10.1093/mnras/252.1.47P)
- Warner, B. 1995, *Cataclysmic variable stars*, Vol. 28
- Washington, J. E., Lewis, H. M., Anguiano, B., et al. 2021, *ApJ*, 918, 19, doi: [10.3847/1538-4357/ac09ec](https://doi.org/10.3847/1538-4357/ac09ec)
- Wilms, J., Allen, A., & McCray, R. 2000, *Astrophys. J.*, 542, 914, doi: [10.1086/317016](https://doi.org/10.1086/317016)
- Woods, T. E., & Gilfanov, M. 2016, *MNRAS*, 455, 1770, doi: [10.1093/mnras/stv2423](https://doi.org/10.1093/mnras/stv2423)
- Zacharias, N., Monet, D. G., Levine, S. E., et al. 2005, *VizieR Online Data Catalog*, I/297
- Zaritsky, D., Harris, J., Thompson, I. B., & Grebel, E. K. 2004, *Astron. J.*, 128, 1606, doi: [10.1086/423910](https://doi.org/10.1086/423910)
- Zaritsky, D., Harris, J., Thompson, I. B., Grebel, E. K., & Massey, P. 2002, *Astron. J.*, 123, 855, doi: [10.1086/338437](https://doi.org/10.1086/338437)

This figure "orcid-ID.png" is available in "png" format from:

<http://arxiv.org/ps/2209.02524v1>